FLEXIBLE PEROVSKITE SOLAR CELL ON METAL PLATE

by

Seongha Lee

B.S, Keimyung University, 2014

Submitted to the Graduate Faculty of

Swanson School of Engineering in partial fulfillment

of the requirements for the degree of

Master of Science

University of Pittsburgh

2017

UNIVERSITY OF PITTSBURGH

SWANSON SCHOOL OF ENGINEERING

This thesis was presented

by

Seongha Lee

It was defended on

March 30, 2017

and approved by

Jung-Kun Lee, PhD, Associate Professor

Department of Mechanical Engineering and Material Science

Qing-Ming Wang, PhD, Professor

Department of Mechanical Engineering and Material Science

Sangyeop Lee, PhD, Assistant Professor

Department of Mechanical Engineering and Material Science

Thesis Advisor: Jung-Kun Lee, PhD, Associate Professor

FLEXIBLE PEROVSKITE SOLAR CELL ON METAL PLATE

Seongha Lee, M.S.

University of Pittsburgh, 2017

I report highly bendable and efficient perovskite solar cells (PSCs) that use thermally oxidized layer of Titanium (Ti) metal plate as an electron transport layer (ETL). The power conversion efficiency of flexible PSCs reaches 14.9 % with short-circuit current density (J_{sc}) of 17.9 mA/cm^2, open circuit voltage (V_{oc}) of 1.09, and fill factor (ff) of 0.74. Moreover, the Ti metal based PSCs exhibit a superior fatigue resistance than ITO/PEC substrate, which flexible PSCs is maintained at 100 % of their initial PCE even after PSCs are bent at R= 4 mm, and 1000 times. This excellent performance of flexible PSCs is due to high crystalline quality and low oxygen vacancy concentration of TiO_2 layer. The concentration of oxygen vacancies in the oxidized TiO_2 layer of Ti metal surface controls the electric function of TiO_2 as ETL of PSCs. A decrease in the oxygen vacancy concentration of TiO_2 layer is critical to improving the electron collection efficiency of ETL. Our results suggest that Ti metal based PSCs possess excellent mechanical properties which can be applied to the renewable energy source of wearable electronics.

TABLE OF CONTENTS

LIST OF TABLES

LIST OF FIGURES

NOMENCLATURE

PSC   Perovskite solar cell

ETL   Electron transport layer

J_{sc} Short-circuit current density

V_{oc} Open-circuit voltage

FF   Fill factor

ITO   Indium doped tin oxide

PET   Polyethylene Terephthalate

PEN   Polyethylene Naphthalate

ALD   Atomic Layer Deposition

PCE   Power covert efficiency

HTL   Hole Transport Layer

Ti   Titanium

R_{sh} Shunt Resistance

R_s Series Resistance

ρ Resistivity

HTM   Hole Transport Materia

J-V   Current density-voltage

I_{sc}	Short-circuit current
IPCE	Incident photon-to-current efficiency
R	Curvature
D	Diffusivity
EQE	External Quantum Efficiency
FTO	Fluorine doped tin oxide
TCO	Transparent conducting oxide
DSSC	Dye-sensitized solar cell
DC	Direct current
AC	Alternate current
XPS	X-ray Photoelectron Spectroscopy
Si	Silicon
EHP	Electron-hole pair
VB	Valence band
CB	Conduction band
EF	Fermi energy level
NW	Nanowire
NP	Nanoparticle

ACKNOWLEDGMENT

1.0   INTRODUCTION

A general device structure of PSCs with very high PCE is similar to the *n-i-p* type semiconductor solar cells.[1][2][3][4] The perovskite layer is coated on mesoporous or planar TiO_2 that is placed on the rigid transparent conducting oxide (TCO) substrate such as ITO/glass or FTO/glass. Recent studies show that the highly crystalline TiO_2 is necessary as an electron transport layer (ETL) of high efficiency PSCs.[5][6] Therefore, it is needed to anneal TiO_2 layer at high temperature (*ca.* 500 ºC) before the perovskite layer is coated. However, this common process cannot be applied to the flexible polymer substrates such as polyethylene terephthalate (PET) and polyethylene naphthalate (PEN) that are suitable for the power source of wearable electronics. To address this problem, researchers have numerously reported the fabrication of *n*-type materials at low temperature (under 150 ºC).[7][8][9] For example, B. J. Kim *et al.* deposited the low-temperature processed TiO_x compact layer on ITO/PEN substrate by using atomic layer deposition (ALD), achieving high PCE with 12.2% at 80 ºC.[10] D. Yang et al. reported that the amorphous TiO_2 grown by magnetron sputtering at room temperature increases PCE of PSCs on ITO/PEN to 15.07%.[11] In recent years, flexible PCSs of the inverted structure (*p-i-n*) are designed. The flexible inverted PCSs are composed of NiO_x, PhNa-1T, or PEDOT: PSS as *p*-type hole transport layer (HTL) on ITO/polymer substrate.[12][13][14] The PCE of the flexible inverted PSCs reaches 14.7% which is not as good as the best performing PSCs on the rigid substrate (> 22%).[13] Recent results indicate that there is limitation in increasing PCE of

flexible PSCs without using high-temperature annealing of TiO_2 layer. In addition, the mechanical strength of PSCs on ITO/polymer substrate weak due to low fatigue resistance of thick ITO layer (*ca.* 200 nm). Since Poisson's ratio of ITO is smaller than that (>0.3) of $CH_3NH_3PbI_3$, ITO is less bendable than $CH_3NH_3PbI_3$.[14] Consequently, as PSCs are bent repeatedly, a crack is formed in ITO layer and propagates through the perovskite layer, resulting in the degradation of PSCs.

There are several alternatives to ITO/plastic substrates such as graphene coated polymers, surface treated metal plates and metal meshs.[15][16][17] Among these alterative materials, metal plate can be an attractive candidate, due to the capability of high temperature annealing, low manufacturing cost, and excellent mechanical property.[18] In fact, there are several studies on PSCs of titanium (Ti) metal substrate and transparent top electrode.[19][20][21] However, the maximum PCE of PSCs built on the surface oxidized TiO_2 /Ti substrates was only 13.1 % which is much smaller than PCE of other flexible PSCs.[21] Furthermore, there has been no systematic research on the structure and property of TiO_2 layer that is produced by oxidizing Ti plates.

Here, we report highly bendable PSCs with high PCE employing thermal oxidation of Ti metal plate. The role of surface oxidized Ti metal in PSCs was systematically investigated as a function of thermal annealing condition. The concentration of oxygen vacancies in the oxidized TiO_2 layer of Ti metal surface is found to control the electric function of TiO_2 as ETL of PSCs. We demonstrate that a decrease in the oxygen vacancy concentration of TiO_2 layer is key to improving the electron collection efficiency of ETL. The highest PCE of flexible PSC on Ti plate is 14.9 % with short-circuit current density (J_{sc}) of 17.9 mA/cm^2, open circuit voltage (V_{oc}) of 1.09, and fill factor (*ff*) of 0.74 under AM 1.5 illumination. This highest value of *ff* and V_{oc} is due to high crystalline quality and low oxygen vacancy concentration of TiO_2 layer. Moreover, the Ti

2

metal based PSCs exhibit a superior fatigue resistance than ITO/PET substrate, which flexible PSCs is maintained at 100 % of their initial PCE even after PSCs are bent at R= 4 mm, and 1000 times. This suggests that Ti metal based PSCs possess excellent mechanical properties which can be applied to the renewable energy source of wearable electronics.

2.0   BACKGROUND INFORMATION AND LITERATURE REVIEW

This chapter is mainly introducing some common knowledge of perovskite solar cell. Basic concepts and behaviors such as properties, structures, and characterization of perovskite solar cell will be introduced. In order to have a better understanding on perovskite solar cell, which is the core of this thesis, a brief introduction will also be included in this chapter.

2.1   SOLAR ENERGY AND SOLAR CELLS

One of the most important global issues are supply of clean and sustainable energy because of destroyed environment and increased energy consumption on the earth. A greater portion of today's energy demand over 85% is fulfilled by fossil fuel based resources but this resource address consequent severe impact on climate changes, pollution and energy insecurity. Moreover, since fossil fuel is finite energy and energy demand in the world is expected to increase 2 times by 2050, an additional energy resources are essential to be satisfied with energy consumption and security in the world. The renewable energy resources such as solar and wind which are cost effective and abundant in nature are fairly distributed over the world. These nature resources have highest potential to contribute and provide towards energy demand. They can also eliminate the environment issues associated with the use of fossil fuels. Over the past

decade, a lot of studies have been reported about renewable resource energy such as wind, water, and sunlight resources.

Among the renewable and finite energy resources, solar energy is the cleanest and most abundant renewable energy source available to meet world's primary energy demand as shown in Figure 2.1. The year supply of solar energy is 30 times larger than the total planetary reserves of coal and 1500 times larger than the current planetary energy consumption.
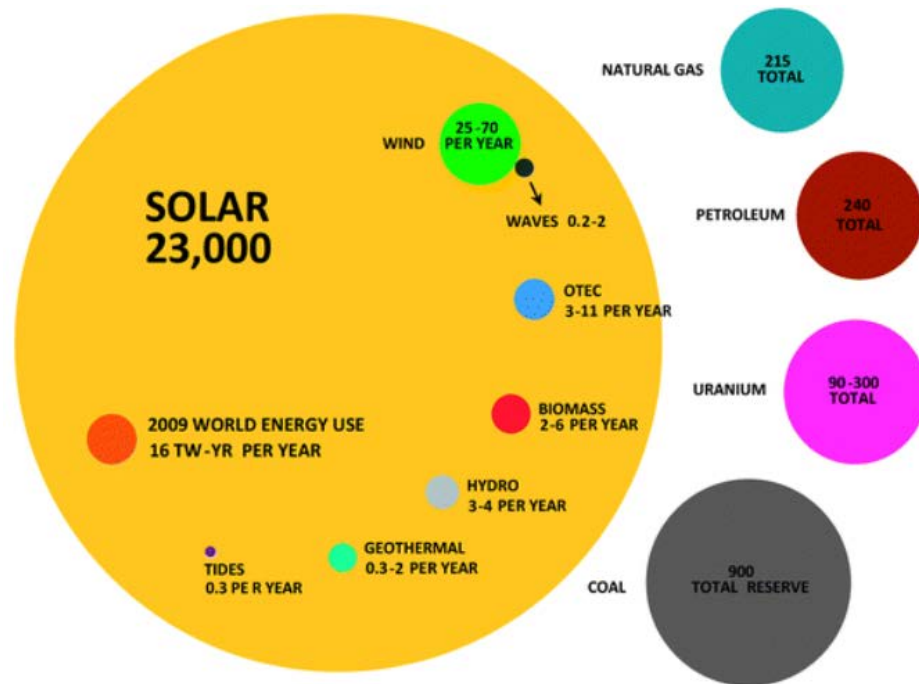
Figure 2.1. Comparison of finite and renewable planetary energy reserves (Terawatt-years). Total recoverable reserves are shown for the finite resources. Yearly potential is shown for the renewables.[22]

Modern technology and researchers have harnessed this energy for a variety of uses, including generating electricity, providing light or a comfortable interior environment, and heating water for domestic, commercial, or industrial use.

There are several ways to harness solar energy such as photovoltaics, heating and cooling, and passive solar. The photovoltaics (PV), which use mechanical or electrical devices that convert

the sun's heat or light to another form of usable energy are the object of steadily growing interest in both academic and industrial areas nowadays.

2.1.1   Introduction to Solar Cells

Since the sun, which is renewable or sustainable energy source, has provided with plenty of energy, scientists and engineers have utilized solar radiation directly by converting it into useful heat or electricity. Two main types of solar energy systems are in use today such as photovoltaics, and thermal systems.

The energy of solar radiation is directly utilized in mainly two forms. Firstly, direct conversion into electricity that takes place in semiconductor devices called solar cells. In general, this is often described as a photovoltaic energy conversion because it is based on photovoltaic effect. Secondly, it requires accumulation of heat in solar collectors.

The photoelectric effect is the emission of electrons or other free carriers at the junction of two different materials in response to visible or other radiation. Electrons emitted in this manner can be called photoelectrons. The phenomenon is commonly studied in electronic physics, as well as in fields of chemistry, such as quantum chemistry or electrochemistry. The whole field of solar energy conversion into electricity is denoted as the "photovoltaics".

There are three types solar cells which are divided from solar technology. The first one is crystalline silicon solar cells, the second one is thin film solar cells and the last one is molecular absorber solar cells. Examples of the last one are polymer solar cells, dye-sensitized solar cells (DSCs), and recently perovskite solar cells.
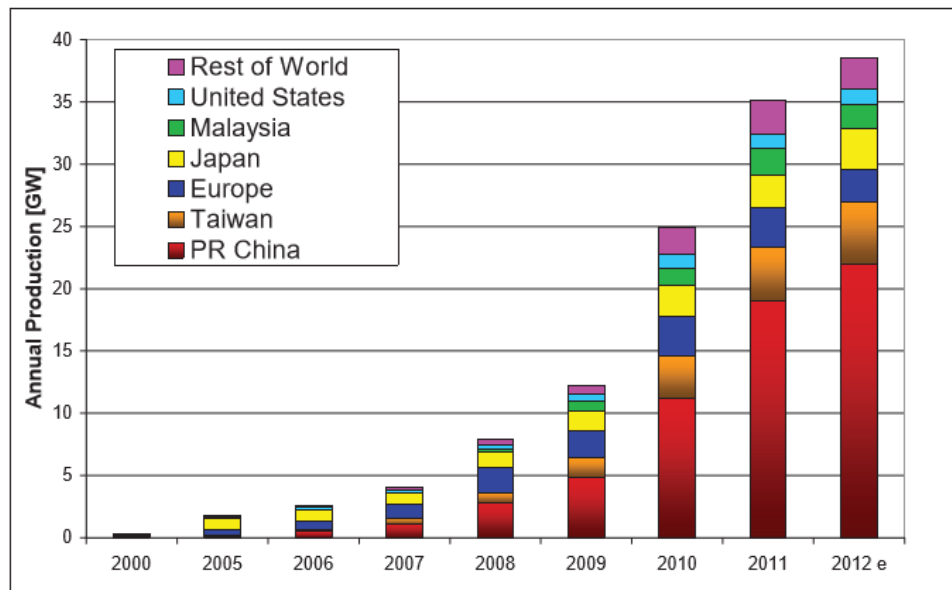
Figure 2.2. Production of world photovoltaic cell/module production.[23]

Since photovoltaic has greatly gained attention in the area of both industry and academic, the production of photovoltaic is significantly increased from 2010 to 2012 as shown above Figure 2.2. The growth rate of production in photovoltaic market was on average over 40%.

Although PV solar energy has a lot of advantages such as environmentally friendly, no noise, no moving parts, no emissions, long life time etc., there are still required improvements for large scale applications and high initial costs that overshadow the low maintenance costs. Moreover, PV generates direct current which means that it needs energy storage such as batteries as an off-grid application.

2.1.2 Perovskite Solar Cell

A perovskite solar cell is a type of solar cell. This includes a perovskite structured compound, most commonly a hybrid organic-inorganic lead or tin halide-based material, as the light-

harvesting active layer. Perovskite materials such as methylammonium lead halides are cheap to produce and relatively simple to manufacture. Perovskites possess intrinsic properties like broad absorption spectrum, fast charge separation, long diffusion distance of electrons and holes, long carrier separation lifetime. These properties of perovskite materials make them very promising materials for solid-state solar cells, called perovskite solar cells.
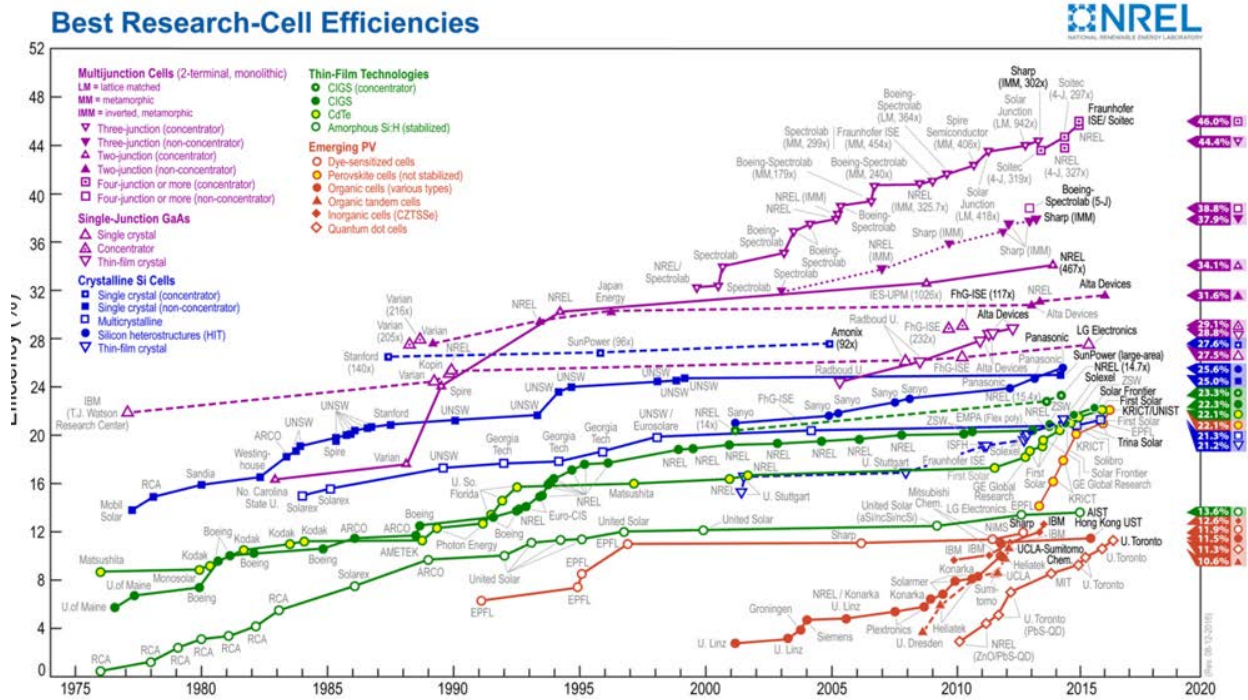
Figure 2.3. Best research-cell efficiency[24]

Since perovskite solar cells with good properties has gained attention in the field of photovoltaic, it aims to increase the efficiency and lower the cost of solar energy. As shown above Figure 2.3, power conversion efficiency of perovskite solar cells has dramatically increased from 2013 to now. Exceptional power conversion efficiencies already exceeded 20% in the lab,[25] and relative ease of fabrication. A big advantage of perovskite solar cells that have exceeded conventional solar technology is that they can react to various wavelengths of light. It

means that they can convert more of the sunlight that reached them into electricity, result in high efficiency.

Moreover, they offer flexibility, semi-transparency, and light-weight. Naturally, these additional properties can create many more applications for solar cells. However, perovskite solar cells still face several challenges such as stability and environmental issue, which need to be improved.

2.1.2.1 Development of Perovskite Solar Cell

These perovskite materials have gained attention for many years. In 2009, Miyasaka et al. reported apparently the first incorporation into a solar cell.[26] It was dye-sensitized solar cell architecture, and eventually achieved a power conversion efficiency of 3.8% using thin perovskite layer as a light absorber on mesoporous TiO_2 as an electron transport layer. However, this dye-sensitized solar cell was only stable for five minutes because of a liquid corrosive electrolyte. After that, Park et al. developed the same dye-sensitized concept, achieving 6.5% PCE in 2011 by applying TiO_2 surface treatment before deposition.[27] Perovskite nanoparticles exhibited better absorption but electrolyte was used to dissolve it, which results in a degradation of performance.

Henry Snaith and Mike Lee from the University of Oxford reported success improvement of perovskite with a solid-state hole transport layer such as spiro-OMeTAD with four additional developments. One of these developments was the mixed-halide $CH_3NH_3PbI_{3-x}Cl_x$, resulting in better stability and carrier transport than its pure iodide. A second was the use of the solid-state hole transporter such as and without the mesoporous TiO_2 layer in order to transport electrons.[28] They achieved almost 10% power conversion efficiency with the 'sensitized' TiO_2. By applying the mesoporous TiO_2 with Al_2O_3, they confirmed that open-circuit voltage was

increased. As a result, they got a relative improved efficiency of 3-5% more than that of the mesoporous TiO$_2$. These experiments demonstrated that a scaffold is not needed for electron extraction and the perovskite itself could also transport holes, as well as electrons.[27] A simple planar structure with no mesoporous scaffold was achieved over 10% of power conversion efficiency.

In 2013, Grätzel's group improved the morphology of perovskite by using scaffold TiO$_2$ and two-step iodide. They got an exceeding 15% efficiency by a two-step solution processing.[3] Snaith's group reported similar results without scaffold TiO$_2$ and fabricated planar solar cells by thermal evaporation, also achieving more than 15% efficiency as almost the time. [29] Docampo et al. also reported possible fabrication of perovskite solar cell, an 'inverted' configuration with the hole transporter below and the electron collector above the perovskite planar film.[7]

Yang Yang at UCLA reported reverse-scan efficiency of 19.3% with the planar thin-film of perovskite using a range of deposition.[30] At the 6th World Conference on Photovoltaic Energy Conversion in Kyoto, Japan, a single-junction perovskite solar cell was mentioned with a power-conversion efficiency of 24% without further details in .

Recent works are focus on improvement of long-term stability of perovskite solar cell for commercialization on the PV market. And another problem is toxicity of Pb for adoption of such PV products in consumer or building integrated application. However, diversity of perovskite solar cells such as flexibility and multi-junctions allow market introduction as a new premium product.

2.1.2.2 Preparation Method of Perovskite Solar Cell

High-quality perovskite films require appropriate morphology, uniformity, phase purity, and crystallinity of perovskite for high-performance PV devices. Deposition method, precursor composition, and additive engineering can significantly affect the crystallization and quality of perovskite film.

In solution processing, two method are available. Lead halide (PbI_2) and methylammonium iodide (MAI) can be dissolved in solvent such as *N,N*-dimethylformamide (DMF) and dimethyl sulfoxide (DMSO). After that, it is spin-coated on a substrate, called one-step coating.[28] Subsequent evaporation and convective self-assembly during spin-coating results in dense layers of well crystallized perovskite material, due to the strong ionic interactions within the material. For the two-step coating method, PbI_2 solution firstly is deposited on a substrate, and then MAI solution is spin-coated on dried PbI_2 film.[25] Two-step process results in more uniform and dense perovskite film by controlling grain size of perovskite through varying the MAI solution concentration, comparing with one-step coating. However, this process has roughness surface of perovskite film, which results in poor performance, from large perovskite grain size. For advanced engineering of one-step process, it requires the addition of other chemicals such as GBL and DMF using for homogenous layer and uniform thickness of perovskite film, called solvent engineering, because simple spin-coating does not yield homogenous layers as a result of the presence of voids, platelets, and other defects in the layer, which would hinder the efficiency of a solar cell.[28] Moreover, the precursor solution, PbI2 and MAI in DMF, with DMSO forms smooth and homogenous perovskite film, called additive engineering.[2] This additives controls balanced nucleation and grain growth rate of perovskite film, preventing from large perovskite grain with a significant number of voids.

11

In thermal vapor deposition, vapor phase deposition is widely used for fabricating high-quality semiconductor thin films with uniform thickness and composition. Mitzi et al. demonstrated this process in 1999[31] and Snaith et al. modified the technique for dual-source thermal evaporation.[29] After thermal evaporation for perovskite film, the deposited film was annealed at a temperature of around 100 °C in the N2-filled glove box, resulting in extremely uniform and pin-hole free.[29] This technique has an advantage over solution processing, which allows it to deposit sequence layer by layer vacuum sublimation.[32] Additionally, vapor deposited techniques result in less thickness variation than simple solution processed layers. However, this technique requires precise control over temperature during thermal evaporation due to low thermal stability.

Both processes of solution and vapor deposition are promising due to low fabrication cost and simple process than silicon solar cells. Vapor deposition or vapor assisted techniques reduce further solvents for high quality perovskite film, resulting in the risk of solvent remnants for environment.

2.1.2.3 Architecture of Perovskite Solar Cell[33]

According to the conventional perovskite solar cell, the mesoscopic n-i-p structure is the original architecture of the perovskite PV devices and is still widely used to fabricate high-performance devices as shown below Figure 2.4 (a). The structure in Figure 2.4 consists of a TCO and FTO cathode with a 50 to 70-nm thick compact TiO_2 as an ETM. A 150 to 300 nm thick mesoporous metal oxide is filled with perovskites, and then 300 nm of perovskite is deposited by spin-coating. A 150 to 200 nm thickness of 2,2',7,7'-tetrakis(N,N-di-p-methoxyphenylamine)-9,9'-

spirobifluorene (spiro-MeOTAD) as a hole transport layer is formed on the perovskite later, which is followed by 50 to 100 nm of a metal anode such as Au or Ag.
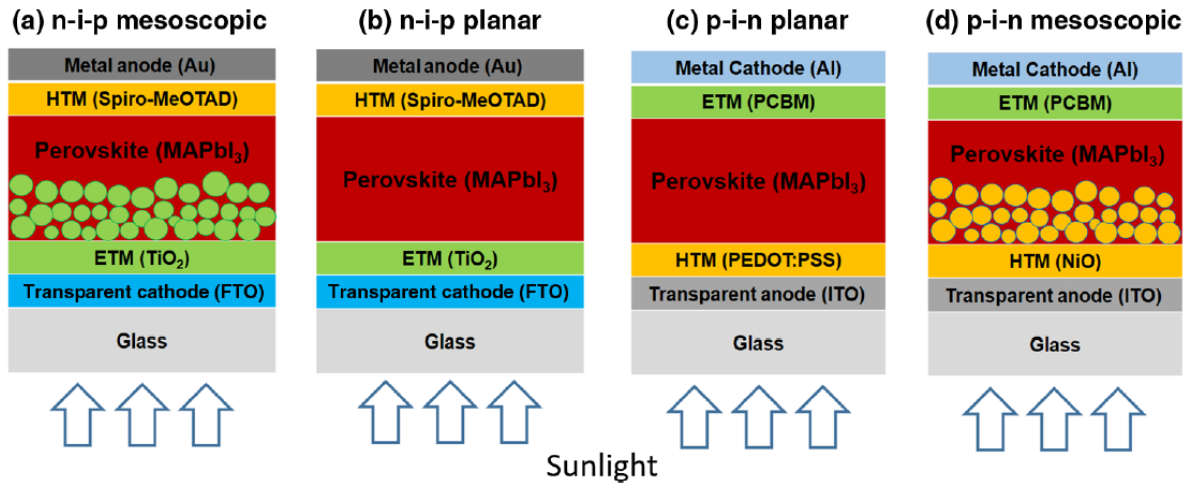
Figure 2.4. Schematic diagrams of perovskite solar cells in the (a) n-i-p mesoscopic, (b) n-i-p planar,(c) p-i-n planar, and (d) p-i-n mesoscopic structures.[33]

The mesoscopic layer in this structure enhances charge collection by decreasing the carrier transport distance, preventing direct current leakage between the two selective contacts and increasing photon absorption due to light scattering. Accordingly, the original mesoscopic perovskite devices used a thick porous layer less than 500 nm to efficiently absorb the incident light.[1][34] But because the grain growth of the perovskites is confined by the pores in the structure, a significant amount of the material is present in disordered and amorphous phases.[35] This leads to relatively low open-circuit voltage (V_{OC}) and short-circuit current density (J_{SC}).[36] Surprisingly, thin the mesoporous layer to 150 to 200 nm results in improved device efficiency due to enhanced crystallinity in the perovskite absorber. Additionally, the pore filling fraction and morphology of the perovskites is critically dependent upon the thickness of mp-TiO$_2$.[37][38] When the porous layer thickness is reduced to less than 300 nm, the pore filling fraction is increased and a perovskite capping layer forms on top of the porous structure. Complete pore

13

filling accompanied by formation of a capping layer assures high charge transport rates and high collection efficiencies at the TiO$_2$ interface. Once the charges are separated, recombination pathways between electrons in the TiO$_2$ and holes in the HTM are blocked due to the relative positions in energy of the respective conduction and valence bands.[37] Consequently, the mesoscopic n-i-p structure is the most popular structure reported in the literature. The previous record efficiency value, which was 20.2%, was measured from a cell formed in the mesoscopic structure that had discrete perovskite nanocrystals embedded in the porous ETM film with an overlaying continuous and dense perovskite capping layer.[39]

The planar n-i-p structure in Figure 2.4 (b) is the natural evolution of the mesoscopic structure. A larger area mesoporous ETM was initially considered critical for high-efficiency perovskite devices because hole extraction at the HTM interfaces is significantly more efficient than electron extraction at the ETM interfaces.[40] However, by delicately controlling the formation of the perovskite absorber, and the interfaces among the perovskite, carrier transport layers, and electrodes, high efficiencies can now be achieved without a mesoporous layer.[30] To date, the best planar n-i-p device showed a 19.3% efficiency after careful optimization of the electron selective indium tin oxide (ITO)/TiO$_2$ interfaces.[30] Although the planar n-i-p perovskite solar cell usually exhibits enhanced V_{OC} and J_{SC} relative to a comparative mesoscopic device processed with the same materials and approach, the planar device usually exhibits more severe $J - V$ hysteresis. Thus, the state-of-the-art n-i-p devices usually include a thin mesoporous buffer layer under 150 nm filled and capped with the perovskite.[39]

When the deposition order is changed and the HTM layer is deposited first, the device is fabricated in the p-i-n structure, called inverted structure of perovskite solar cell, in Figure 2.4 (c). In this case, the p-i-n type perovskite device is built on a 50 to 80 nm p-type conducting polymer

such as poly(3,4-ethylenedioxythiophene) poly(styrene-sulfonate) (PEDOT:PSS), which is deposited on ITO-coated substrates. After depositing a 300 nm intrinsic perovskite thin film, the device is completed with a 10 to 60 nm organic hole-blocking layer [6,6]-phenyl C61-butyric acid methyl ester (PCBM) and a metal cathode such as Al or Au. Early device design utilized a perovskite and fullerene (C60) donor–acceptor pair, which is typical in OPV.[41] In fact, the commonality in structure has allowed OPV researchers to easily move into the field of perovskites. As the field has advanced, the organic acceptor has been omitted in favor of an ETM layer, leaving the planar perovskite absorber sandwiched between two opposite organic charge transporting materials.[42] Recently, the efficiency of the planar p-i-n device has improved significantly due to the use of more advanced material preparation methods, such as a multicycle solution coating process, and a best efficiency of 18.9% was achieved.[43] Further development of the p-i-n device structure has expanded the selective contact options from organic to inorganic materials. For example, NiO and ZnO/TiO$_2$ layers have recently been used for the hole and electron selective contacts, respectively, which makes the perovskite device distinct from its organic counterpart.[44][45] Inorganic charge extraction layers such as NiMgLiO and TiNbO2 have been used to fabricate large-area up to 1 cm^2, high-efficiency perovskite solar cells, which are 15%, representing a potentially important step in the path toward commercialization.[44] The use of oxide HTMs also allows for construction of the mesoscopic p-i-n device structure in Figure 2.4 (d), in which NiO/mp-Al$_2$O$_3$ or c-NiO/mp-NiO are used as the HTM.[46][47] The best mesoscopic p-i-n device with a nanostructured NiO film demonstrated a 17.3% efficiency.[48]

2.2   THE PROPERTIES OF PEROVSKITE

2.2.1   Crystal Structure

Perovskite is a common name of crystal structure with a general chemical formula of ABX_3, where X is an anion and A and B are cations of different sizes as shown in Figure 2.5. This structure refers to the crystal structure of calcium titanate ($CaTiO_3$) which was discovered by Gustav Rose and so it was named after Russian mineralogist, Lev Perovski. In the ABX_3 compound, B represents halide atoms whereas A represents cations which can be either metal or hydrocarbon.
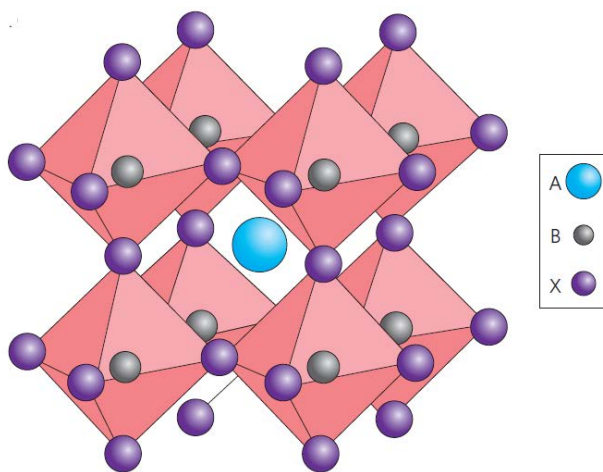
Figure 2.5. Perovskite crystal structure.[49]

In general, there are several types of perovskite compounds, both inorganic based and organic based, with a variety of properties such as antiferromagnetic, piezoelectric, thermoelectric, semiconducting, conducting, and superconducting. Organo-metal halide perovskites (OMHPs) are a group of materials with the formula AMX_3 where A is an organic

cation ($CH_3NH_3^+$ or $NH_2CH_3NH_2^+$), M is a divalent metal cation (Pb^{2+} or Sn^{2+}), and X is a monovalent halide anion (I^-, Br^-, or Cl^-). The use of OMHP material in solar cell applications has gained more and more interest over the last few years. This was attributed to the fact that the 1.55 eV band gap ofMAPbI$_3$ is nearly ideal for single-junction solar cells exposed to the solar irradiance spectrum, and it can be continuously varied in the range from 1.5 to 2.3 eV by exchanging the organic and halide ions. In addition, electronic properties of perovskite can be adjusted by tailoring made chemical structure of the material. In the case of OMHPs, experimental results from photoluminescence quenching technique[50] revealed that diffusion length of the photo generated exciton is a long as 1 μm which results from the high electron and hole mobility in the range of 10 to 60 cm^2 $V^{-1}s^{-1}$ and the long carrier life time (~100 ns). This means that the exciton from perovskite has less chance to have an experience of recombination which can allow open-circuit voltage over 1 V to be achieved.

2.2.2 Working Principle of Perovskite Solar Cell[51]

Light absorption, charge separation, charge transport, and charge collection are general solar cell working processes. In order to construct them, light harvesters should be selected and their opto-electronic properties investigated. For instance, a p-i-n junction is required in case the light harvester is an intrinsic semiconductor, while a p-n junction is needed if the light harvester possesses an n-type or p-type property, because n- or p-types can transfer electrons or holes to the light harvester. Organo-metallic perovskite materials can be applied to either p-i-n junction or p-n junction types, since they have balanced charge transport properties. Electron and hole transport properties were reported for $CH_3NH_3PbI_3$ prepared by different synthetic methods using a $CH_3 NH_3I + PbI_2$ mixture[40] and a $3CH_3NH_3I+PbCl_2$ mixture,[52] where X-ray

diffraction patterns were indexed as tetragonal $CH_3NH_3PbI_3$ regardless of the preparation method. The electron and hole diffusion lengths were estimated to be 1[nm and 100 nm, respectively, for the samples prepared from the former method, while longer diffusion lengths of 1069 nm for electrons and 1213 nm for holes were measured for the sample prepared using the latter method. The difference in diffusion length depending on preparation method is likely to be due to quality of the perovskite layer, such as crystallinity or grain size. Electron beam-induced current (EBIC) imaging studies of $CH_3NH_3PbI_3$ layers prepared from PbI_2 and $PbCl_2$ sources.
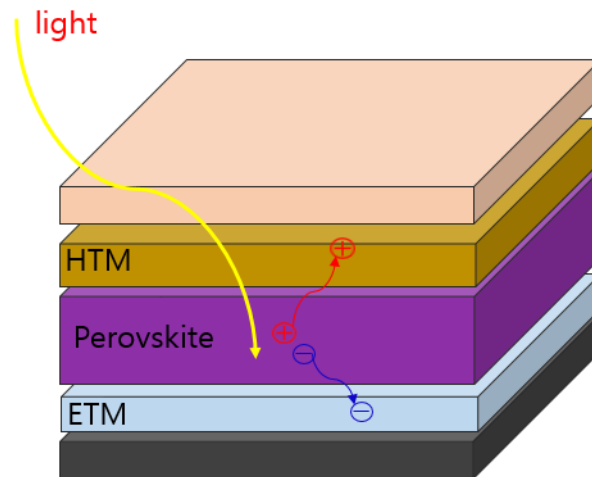
Figure 2.6. Schematic of common P-i-N junction.

2.3   DIRECTION OF PEROVSKITE SOLAR CELL

2.3.1   Stability

One of big challenges for perovskite solar cells is the long-term stability. Environmental influence such as humidity, heat, and light can significantly affect the instability or lifetime of PSCs. Especially, waster-solubility of the organic of the light absorber make perovskite solar cells rapid degradation in moist environment. Several studies about PSCs stability have been reported and some elements have been proven to be important to the PSCs stability.[53][54]

The degradation is caused by the breakdown of perovskite material under moisture and heat stress, which results in the segregation of MAPbI3 into its constituents MAI and PbI2 during the fabrication step.[55][56] The perovskite film is decomposed through thermal stress at a temperature over 110 $^{\circ}$C. Improvement in perovskite solar cell stability by the incorporation of encapsulating the perovskite absorber with a composite carbon nanotubes and an inert polymer matrix is reported to increase the moisture resistance at elevated temperature.[57][58]

In addition, when a mesoporous TiO_2 layer is sensitized with the perovskite absorber, UV light induces instability. The cause for the decline of stability in device performance is related to the interaction between oxygen radicals on the surfaces of TiO_2 and photo-generated holes inside the TiO_2.[36] The coating on the front and back side of perovskite solar cell is demonstrated that it has stabilized excellent stability in terms of power conversion efficiencies during a 180-day in the lab and a real outdoor condition test for more than 3 months.[59] This is because the front coating on the perovskite solar cells prevented the negatively interacting from the UV light of the whole incident solar spectrum by converting it into visible light. In addition, back side coating protects perovskite solar cell from the water permeation.

Also, the PbI$_2$ residue on the surface perovskite film is demonstrated to have a great negative effect on the long-term stability of devices.[60] The organic transport layer with a metal oxide layer stabilized and retained the efficiency of perovskite solar cell for 60 days.[61][45]

2.3.2 High Efficiency

There is limitation to single-junction for high performance. Henry Snaith suggested a major advantage of perovskites that it might be able to utilize their absorption band. This leads to efficiently collects wavelengths of light while the major commercial solar cells such as c-Si and CIGS do not collect.[62] Tandem or multi-junction device can simultaneously absorb light and lose thermalization through utilization higher voltage and lower photocurrent or lower voltage and higher photocurrent. A layer of perovskite film could theoretically be deposited on top of one the standard bulk solar cells such as c-Si. Such a tandem cell would require significant optimization of intermediate layer between perovskite and standard bulk solar cells in order to achieve good lattice matching and charge transfer between ETMs/HTMs.

It is estimated that such a tandem cell, which is combined with perovskite and standard bilk solar cells should has 1.3 times the maximum amount of photons absorbed than that of a single junction by the Shockley-Queisser limit. A tandem perovskite/c-Si cell can achieve good charge transfer, resulting in 29.6% PCE.[62]

2.3.3 Flexibility

Recently, thin film perovskite PVs have gained more interest due to their compatibility such as light-weight and portability in making large area production of flexible modules, which can have

a great effect on lowering the production costs by reduced thickness. In addition, flexible perovskite solar cells are attractive due to low temperature process below 150 ℃, solid-state thin film, and high efficiency.

From the beginning, flexible perovskite solar cells are fabricated on ITO-coated PET substrate with ETM at a low temperature due to a compact TiO2 at a high temperature. For low temperature process of ETM, ZnO nano-particles were deposited at below 150 ℃. Kelly et al. reported an flexible n-i-p structure perovskite solar cell with power conversion efficiency of 10.2%.[8] Recently, flexible perovskite solar cells with a high efficiency was reported by employing a compact TiO2 layer on ITO/PET substrate using atomic layer deposition (ALD),which is also a low temperature process.

However, applied ITO or FTO on flexible substrates have many disadvantages such as degradation of the device performance due to crack formation in ITO/FTO layer during the bending test. Moreover, devices with ITO/PET substrate are unsuitable for providing a high-quality compact TiO2 layer which requires high-temperature. Moreover, ZnO nanoparticles as an ETL showed hysteresis at a different scanning direction. Metal substrates can be a feasible alternative to ITO/PET substrates, which can offer advantages for the fabrication such as high-temperature control.[15] However, the opaque nature of metal substrates hinders the light absorption, so the device will require transparent counter electrode for device performance. In this paper, they used silver nanowire as a counter-electrode, resulting in 7.45% of power conversion efficiency and good bending stability at 97% of initial efficiency.[15]

2.4   CHARACTERIZATION OF PEROVSKITE SOLAR CELL

2.4.1   Power Convert Efficiency and J-V Curve

The current density and voltage are one of the most important characteristics in order to describe the performance of a solar cell. The power conversion efficiency (PCE), also called the efficiency, of a solar cell is defined by the ratio of maximum electrical energy provided by solar cell under sunlight. The power generated can be described as below:

$$P = I * V = (I_L * V) - (V * I_S^{(e^{\frac{qV}{Kt}}-1)})$$

where I_L is photocurrent, V is voltage, I is current output and I_S is saturation current. J-V curve in Figure 2.7 is widely used to determine PCE of solar cells. The PCE is directly related to three parameters of J-V curves: short-circuit current density (Jsc), open-circuit voltage (Voc) and fill factor (FF). Short-circuit current (Isc), which is also known as photocurrent, presents the current of a solar cell generates when it is not linked to any external circuit. Thus, Jsc means diode short-circuit current per area of energy injection from the incident light. As it shows on J-V curve, the Jsc value equals to the current value when V=0. When I=0 on J-V curve, however, the voltage then equals to open-circuit voltage, which is the maximum voltage than generated by a solar cell.
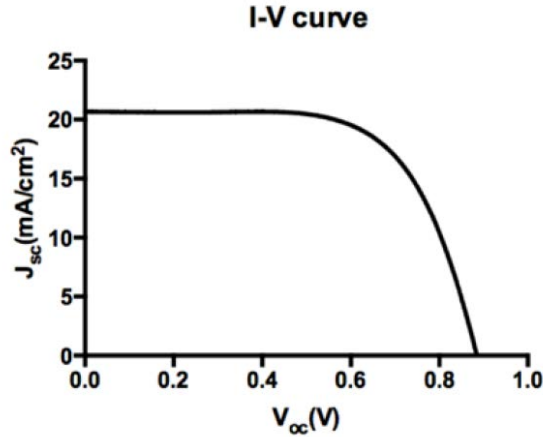
Figure 2.7. Common J-V curve of a perovskite solar cell.

The fill factor (FF) is a geometric factor of J-V curve and defines the ratio of the maximum power to the theoretical power that could be generated. Then, the maximum power (P_{max}) can be generated from a solar cell, a pair of corresponding maximum current (I_m) and maximum voltage (V_m). Thus, the maximum power can be shown as $P_{max}=V_m*I_m$. Based on this relationship, FF is described as below:

$$FF = \frac{V_m * I_m}{V_{oc} * I_{sc}}$$

For real device, series resistance R_S, which results from bulk resistance due to poor attaching between the surfaces of different layers in solar cell and low carrier mobility, can significantly lower the FF and eventually hinder the PCE of solar cell with low charge injection while it reduces the J_{SC} of the cell. A shunt resistance R_{SH} results from leakage current between the two contacts, which leads to a poor device performance. An alternative current path for the light-generated make causes power losses in solar cells. Thus, the equation of the PCE of a solar cell can be given by:

$$PCE = \frac{P_{generated}}{P_{photon}} = \frac{V_{oc} * I_{sc} * FF}{P_{photon}}$$

23

2.4.2 Incident Photon to Current Efficiency(IPCE)

Incident photon-to-current efficiency (IPCE) is an important concept in describing the process of photo power conversion and efficiency of the solar cells to make use of absorbed photons. It is defined as a ratio of the number of electron-hole pairs generated by incident photons to the number of total photons incident on the solar cell. IPCE is a function of the wavelength (λ) of light impingent on the cell. It increases as the number of photons absorbed by solar cell increases and the number of carriers recombined before they reach external circuit decreases. IPCE is calculated by the ratio of photo-generated electrons to incident photons, as shown in Equation:

$$\text{IPCE} = \frac{1240 * I_{sc}}{\frac{I_{photon}}{responsitivity} * \lambda} = \frac{1240 * I_{sc}}{P_{incident\ photon} * \lambda}$$
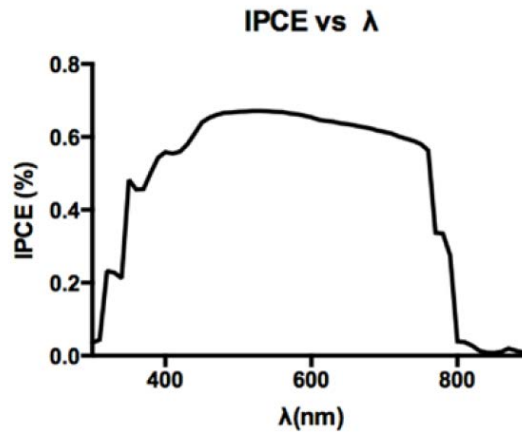
Figure 2.8. Inset of IPCE as a function of incident photon's wavelength.

Most of organic perovskite solar device exhibits 60 to 80% of IPCE value while organic solar cells can reach the highest IPCE value, 100%.

3.0   RESEARCH DESCRIPTION

3.1   HYPOTHESIS

Metal, as an alternative to polymers, can be a viable and attractive substrate candidate for flexible perovskite solar cells because of mechanical properties such as its tremendous endurance at high temperature and flexibility. The primary hypothesis of this thesis is that oxidation of ti substrate can form TiO_2 at high temperature as an electron transport layer and be replaced with other TiO_2 which is formed at low temperature. The secondary hypothesis is that the ti substrate can endure over the course of mechanical bending test. Ti metal based PSCs possess excellent mechanical properties which can be applied to the renewable energy source of wearable electronics.

3.2   OBJECTIVES

The purpose of this thesis is to describe and explain ti oxidation behaviors based on ti substrate and then will be applied to the perovskite solar cell. Therefore, electrical property, micro structure, and surface roughness of TiO_2 will be respectively characterized and show effects to the perovskite solar cell by using shunt resistance, series resistance, I-V curve, and IPCE. For mechanical property of flexible perovskite solar cell, bending test will be conducted.

25

3.3   TASKS

The first task of this thesis is oxidation of ti substrate in air at different temperatures in the range of 400 °C to 700 °C to get TiO_2 as an electron transfer layer and optimized the thickness of TiO_2. The second task is making flexible perovskite solar cells with the optimized thickness of TiO_2 at different temperatures to compare performances and effects of TiO_2 in order to study the behaviors of electron transportation in perovskite solar cell. The third task is doing both mechanical characterization and dynamic photovoltaic measurements.

4.0   EXPERIMENTAL DETAILS

4.1   PEROVSKITE SOLAR CELL FABRICATION

4.1.1   Titanium Substrate Preparation

Perovskite solar cells were fabricated with a structure of Au/Cu/HTM/CH3NH3PbI3/TiO$_2$/Ti. TiO$_2$/Ti substrates were prepared by an oxidation process of Ti foils. (Alfa Aesar, 99.7 wt% purity) were cut in the form of 20 x 20 x 0.025 mm^3 and sequentially cleaned by acetone, deionized (DI) water, and ethanol for 30 minutes, respectively.

4.1.2   Titanium Oxide

After washing, Ti foils were annealed at different temperatures in air to form TiO$_2$ layer at the top of the Ti foils. The thermal growth rate of TiO$_2$ layer was investigated as function of temperature in the range of 400 $^{\circ}$C to 700 $^{\circ}$C for 1 hour. Then, it applied for the same thickness of TiO$_2$ layer.

4.1.3　One Step Perovskite Fabrication

Perovskite layer, the $CH_3NH_3PbI_3$ solution was synthesized by dissolving lead iodide (PbI_2), methyl ammonium iodide (MAI, CH_3NH_3I) and dimethyl sulfoxide (DMSO) with a molar ratio of 1:1:1 in N,N-dimethylformamide (DMF). This synthesized perovskite layer was spin-coated on the top of TiO_2/Ti at 4500rpm for 25 sec with dipped 5ml of ethyl ether. The spin-coated samples were annealed on a hot plate at 65 °C, and then at 100 °C for 1 min and 5 min, respectively.

4.1.4　Hole Transport Material

And then, the HTL solution was deposited by spin-coating from 36 mg of the 2,2′,7,7′-tetrakis[N,N-di(4-methoxyphenyl)amino]-9,9′-spirobifluorene (spiro-OMeTAD) in 500 µl of chlorobenzene with added 14.4 µl of 4-tert-butyl pyridine and 8.8 µl of lithium-bis(trifluoro-methanesulfonyl)-imide (Li-TFSI) solution. 180 mg of Li-TFSI solution was prepared by dissolving in 250 µl acetonitrile.

　　　After the spin coating, a trimming step is added in order to remove the perovskite and HTM coated on FTO side.

4.1.5　Transparent Top Electrode

For transparent top electrode, Au and Cu are used to form the electrodes on the solar cell. It both deposited on perovskite region to form cathode and deposited on FTO side to form anode. This layer is deposited by electron beam deposition method where high intensity electron shoots on a

crucible contains target metal.[63] At very low pressure (<5×10-6 Torr), the metal will be generated by high intensity electron beam and deposited evenly on the holder, where the samples mounted, inside the chamber. Since this method can cover all areas, a mask with electrode pattern is used to cover the sample and expose the electrode area. The deposition rate is 0.05 nm/s and a final thickness are 1 nm-thick of Au and 7 nm-thick.

4.2   I-V CURVE MEASUREMENT

Solar simulator was used to measure J-V curve of perovskite solar cell sample. It can generate sunlight, which contains ultraviolet, visible and infrared light, with different intensity.[64] Since the photocurrent generated by solar cell is a function of incident photon intensity, in order to measure the photocurrent generated under 1 sun's intensity, the light intensity of solar simulator should be calibrated. The 1 sun intensity refers to standard illumination at AM1.5G.[65] The calibration is done by measure the J-V curve of silicon reference solar cell at 1 sun intensity and measure under the solar simulator to obtain another J-V curve. By comparing these two J-V curves, the light intensity of solar simulator can be calculated. The reference J-V curve under 1 sun is shown in Figure 4.1.
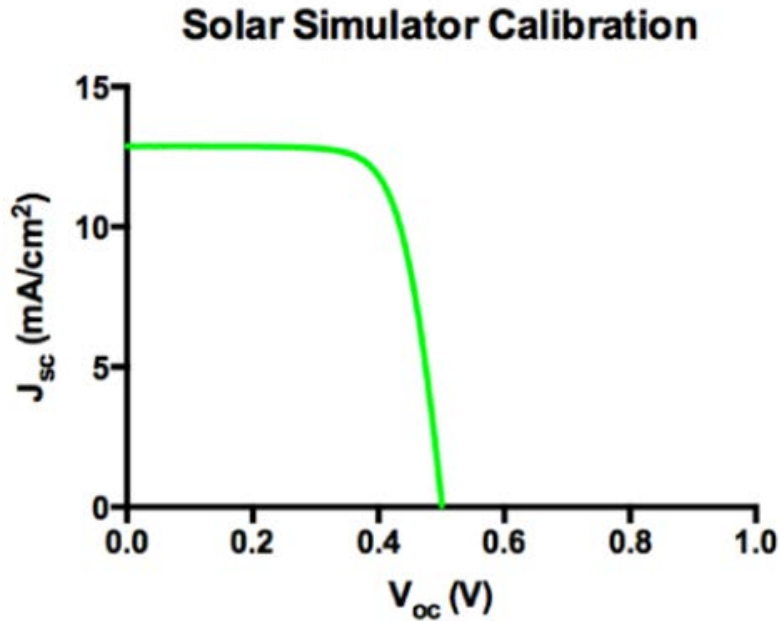
Figure 4.1. The J-V curve of silicon reference solar cell during calibration.

The samples were mounted in I-V holder during the measurement, which has conductive junction points, can link to the electrode on perovskite solar cell sample. The junction points are also linked to electrical measurement sensor and computer, thus the data can be obtained. The area on solar cell is fixed by a metal mask for the calculation of photocurrent density Jsc from photocurrent Isc, which is directly measured from I-V curve measurement. The exposed area is 0.14cm^2. During the measurement, the mask is covered on the sample and exposed area is on the top of electrodes. The corresponding Jsc, Voc and FF are calculated from the curves.

4.3   IPCE MEASUREMENT

Incident photon-to-current efficiency (IPCE) is used to measure the photocurrent generated by perovskite solar cell under different wavelength. The monochromator is used to split light from Xeon lamp to certain wavelength. The wavelength is continuously changing during the measurement in order to obtain photocurrent data in a range. The sample was mounted in light path. Anode and cathode were linked to the detector with a cable. The detector can read photocurrent data and transfer to computer.

5.0   RESULTS AND DISSCUSSION

5.1   SCHEMATIC OF FLEXIBLE PEROVSKITE SOLAR CELL
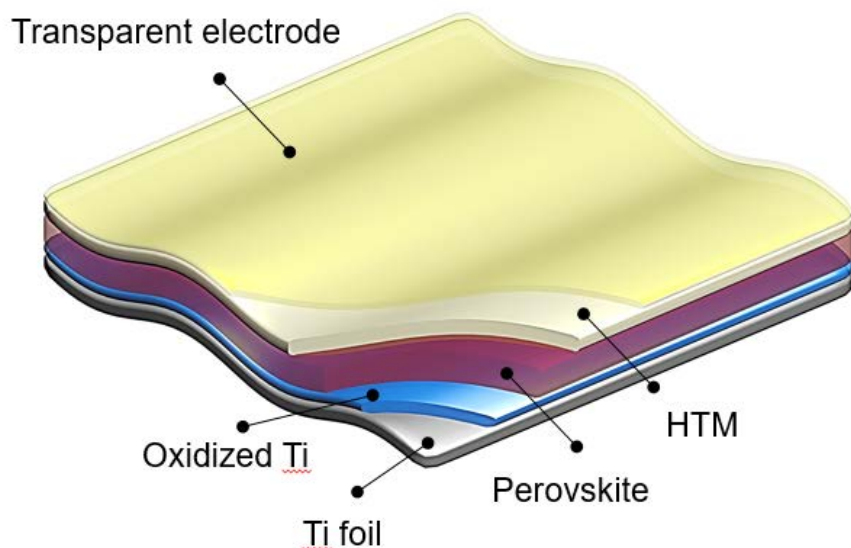
Figure 5.1. Device architecture of the highly flexible cells based on metal substrates tested in this study.

Figure 5.1 presents a structure of flexible perovskite solar cell based on Ti foil (thickness~25μm) with a transparent electrode on top of PSCs. Briefly, the TiO_2 layer was formed by thermal oxidation of Ti foil in air. The defect concentration of TiO_2 layer was controlled by changing annealing temperature. Annealing time was changed to maintain the thickness of the TiO_2 layer. After the thermal annealing, $CH_3NH_3PbI_3$ and HTM were coated sequentially onto the TiO_2/Ti

substrate. On top of HTM, a transparent electrode was formed by coating a very thin metal film (Au ~7 nm/ Cu ~1nm).[66] This structure was designed for highly bendable PSCs with high quality TiO_2 film on Ti metal substrate.

5.2   TRANSPARENT TOP ELCTRODE

The flexible perovskite solar cell on metal plate requires transparent counter electrode that must have high transparency and good conductivity. In this paper, thin metal film of Au/Cu was used as the top electrode.[66] Transmittance of spiro-OMeTAD (200nm) /Cu (1nm)/ Au depending on the thickness of Au from 0 nm to 10nm was simulated by the finite-difference time-domain (FDTD) method in Figure 5.2 (a). As a result, although 1 nm of Cu was the best transmittance as a top electrode, 1 nm Cu and 7 nm Au were chosen because Cu and Au have much better stability in direct contact with perovskite film and thin Cu has low conductivity. In the case of Au, Au atoms lead to formation of Au island through Volmer–Weber growth during thermal evaporation since they agglomerated to each other than to the substrate. 1 nm Cu layer on the surface improves the Au wettability due to much higher surface energy than that of Au. Moreover, 1 nm thickness of Cu and 3 nm of Au improved transparency but, it also significantly increased sheet resistance.[66] As a result, transmittance of the thin metal electrode (1 nm of Cu/7 nm of Au) ranges from 60 to 80 % for visible light. However, since HTL (spiro-OMeTAD) is coated on the top of the perovskite layer, HTL captures solar light of the wavelength smaller than ~420 nm.[67] This leads to relatively lower current density in Figure 5.12.
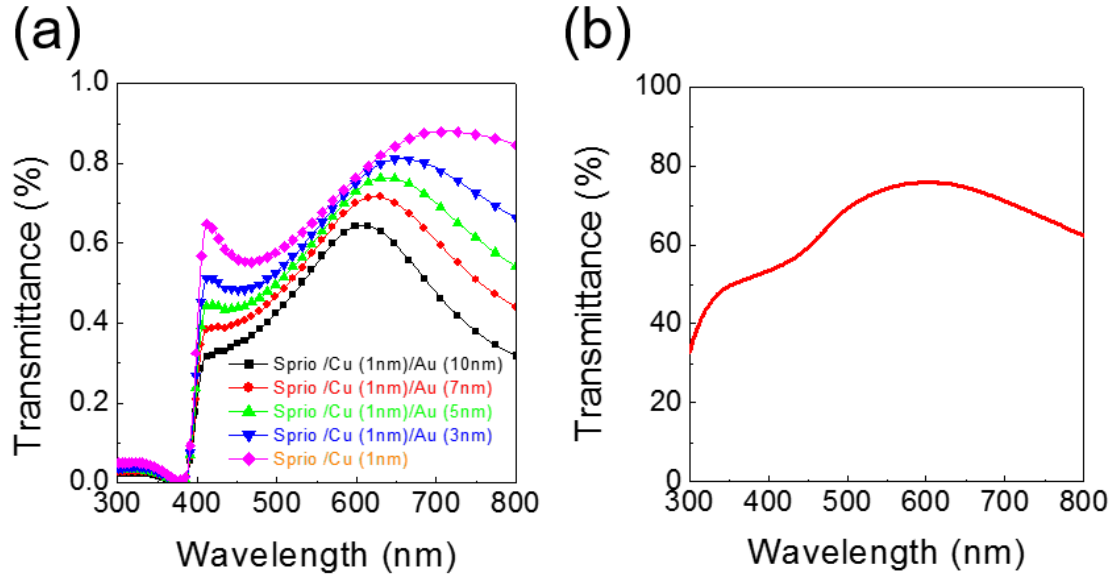
Figure 5.2. (a) Simulated transmittance of spiro-OMeTAD (200nm) /Cu (1nm)/ Au depending on the thickness of Au from 0 nm to 10nm. The simulated transmittance spiro-OMeTAD /Cu/Au film applied to the finite-difference time-domain (FDTD) method to solve the Maxwell equations numerically and simulate the light absorption and transmittance of our layer-by-layer structure. (b) The transmittance of the Cu (1nm)/ Au (7nm) film on the glass.

5.3   TITANIUM OXIDE

5.3.1   Oxidation of Titanium

One of the important experimental variables which can influence the quality and thickness of the oxide layer is annealing temperature. Hence, we systematically investigated the thermal growth rate of TiO_2 layer as function of temperature in the range of 400 °C to 700 °C for 1 hour in air. The thickness of TiO_2 grown at 400 °C, 500 °C, 600 °C, and 700 °C in air for 1 hr was respectively <1 nm, ~70 nm, ~370 nm, > 2 μm measured by ellipsometer. Figure 5.3 shows that

experimental results are in a good agreement with theoretically predicted thicknesses which were

calculated using the oxygen diffusion coefficient at various temperatures.[68]
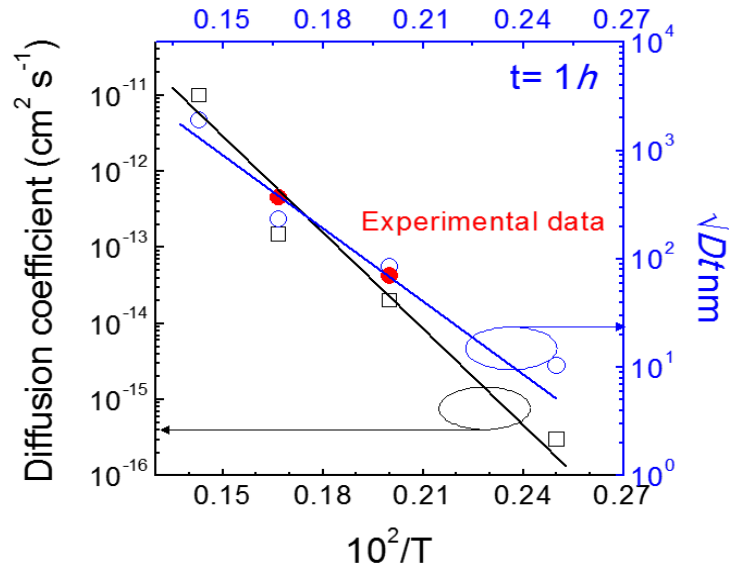
Figure 5.3. The literature diffusion coefficient (black line) and diffusion length of oxygen (blue line) in air for 1

hour at various temperature are shown. Red points are experimentally results of TiO_2 thickness on Ti foil at 500 °C

and 600 °C for 1h.

This difference in the thickness of TiO_2 on Ti is confirmed in ellipsometer which presents a

change in the color of the oxide layer due to the interference in Figure 5.4.[69]
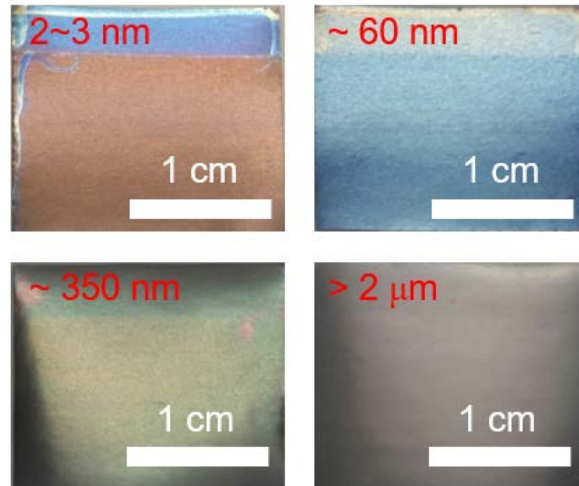
Figure 5.4. The images of oxidized Ti foil show the color change due to interference effect with different temperature.

5.3.2 Surface Roughness of Titanium

To understand the effect of the oxidation temperature of TiO_2 on the PV performance of PSCs, the microstructure, surface roughness, and electrical properties of TiO_2 layer on Ti were analyzed.
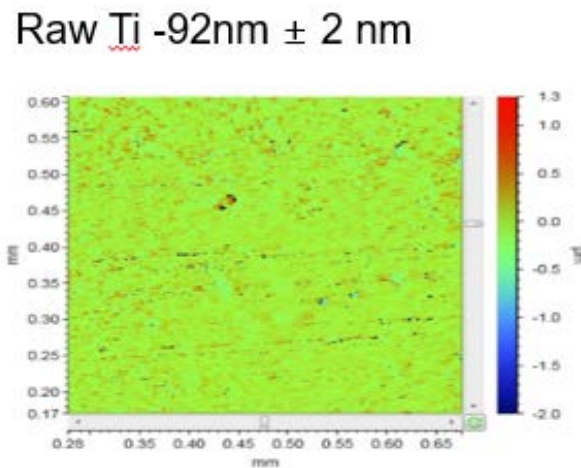
Figure 5.5. Surface roughness of raw Ti by optical profile before oxidization in air.

Figure 5.5 shows optical profile images of the raw TiO_2 surface and the surface roughness of raw Ti is 92 nm. Figure 5.6 shows the oxidized TiO_2 surfaces at different temperatures in the range of 400 °C, 500 °C, 600 °C, and 700 °C in air for 1 hr. The TiO_2 layers which were oxidized at different temperature exhibit the very similar morphology and the surface roughness of all oxide layers is ~150 nm. In addition, there is no microcracks which can be formed by the volume expansion of the oxidation process for TiO_2 surface. Therefore, the effect of the annealing temperature on the PV performance of PSCs cannot be explained by a change in the microstructure of the TiO_2 layer.
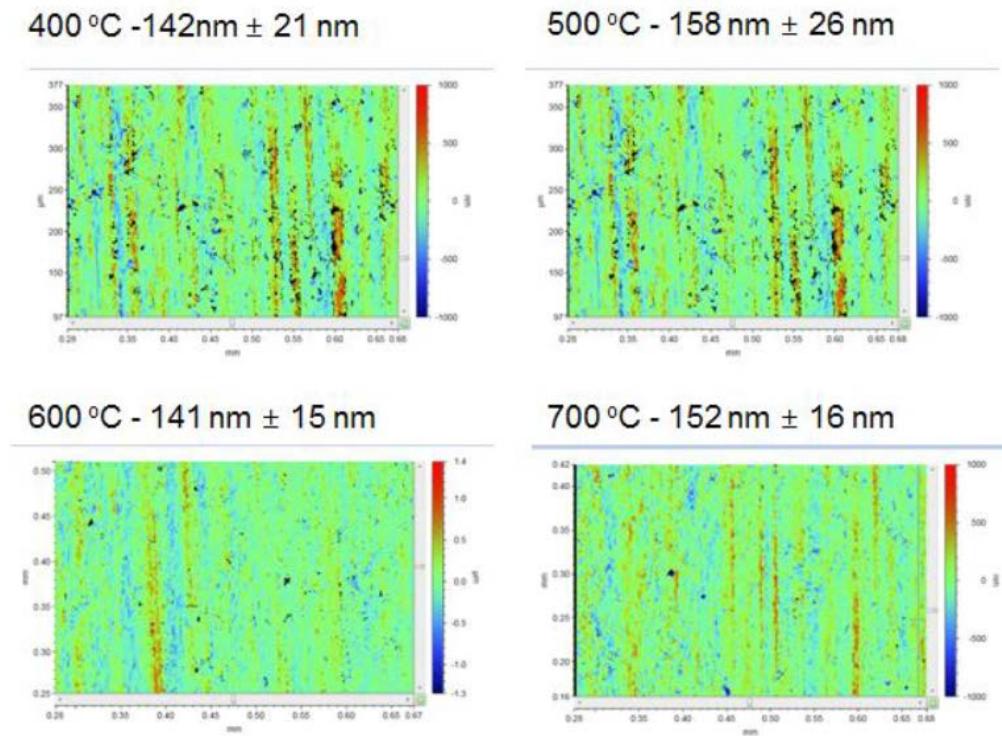
Figure 5.6. Surface roughness of TiO_2 layer measured by optical profile after oxidization in air with the same TiO_2 thickness through different annealing time.

5.3.3 Properties of Titanium Oxide

To examine the effect of the annealing temperature on the electric properties, the electrical resistance of the TiO_2 layer was also measured in Figure 5.7 (a). An electrode configuration of TiO_2 layer for I-V curve measurement is illustrated in inset Figure 5.7 (a).
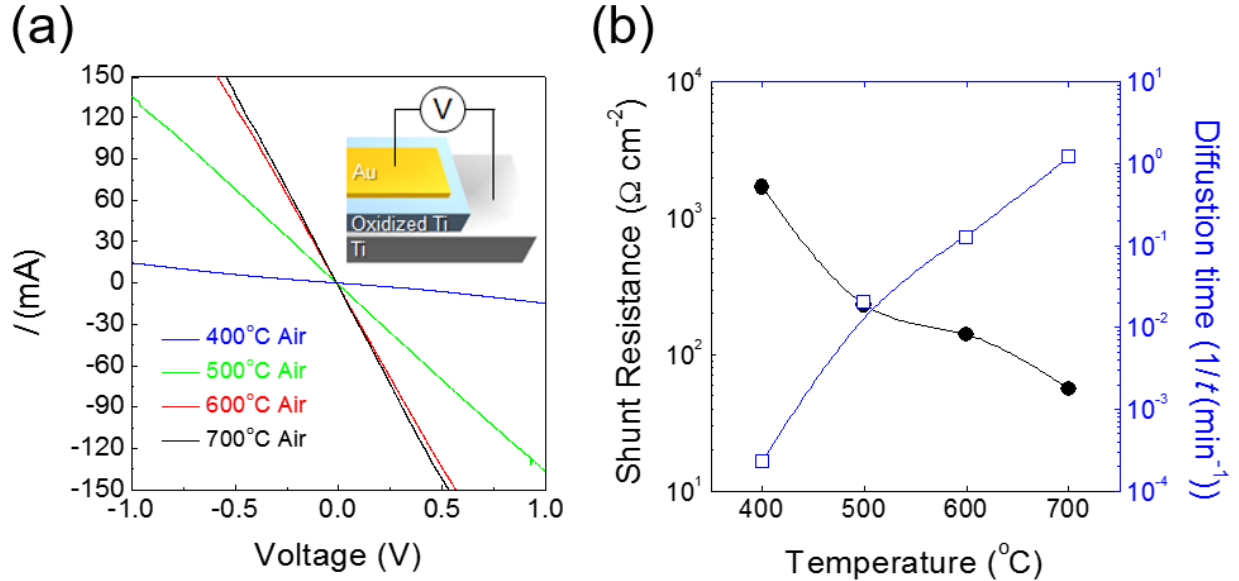
Figure 5.7. (a) The corresponding resistances of oxidized TiO_2 layer with the same thickness depending on different temperatures in air and the measured device structure of the Au/TiO_2/Ti. (b) Changes of representative shunt resistance determined from J-V curves of Au/Cu/HTM/$CH_3NH_3PbI_3$/TiO_2/Ti flexible cells under different oxidation temperature in air and diffusion time calculated at the same condition. The series and shunt resistance was derived in Figure. 5.7 by using a stand diode equation as follow; -dV/dJ at Voc and -dV/dJ at Jsc.

Interestingly, the annealing temperature has a huge impact on the resistance and I-V of TiO_2 layer. TiO_2 layer grown at 400 °C exhibits non-linear I-V curve which was reported in previous studies of highly crystalline TiO_2 films for the resistive random-access memory (ReRAM) application.[70] TiO_2 layer grown at or higher than 500 °C exhibits linear I-V curve and higher temperature annealing significantly decreases the electric resistance of TiO_2 layer.

This suggests that the effect of the oxidation temperature on the PV performance of PSCs is to change the electric property of TiO_2 layer in Figure 5.7 (b). The wide band gap oxide such as TiO_2 is inherently n-type semiconductor. The conductivity of TiO_2 is often controlled by the concentration of defects such as oxygen vacancy and aliovalent impurities (e.g. Mg2+, Nb5+, Ta5+, Al3+ or Y3+).[71][72][73][74][75][76] Given that all TiO_2 films were prepared from a same type of Ti foil, the impurity defect concentrations must be same for all samples. Therefore, the change in the electric of the TiO_2 layer can be attributed to a dependence of the equilibrium oxygen vacancy concentration on temperature. The equilibrium oxygen vacancy concentration exponentially increase as temperature increases.[77] Since the oxygen vacancy works as a shallow donor in TiO_2, more oxygen vacancy at higher temperature means that an increase in the annealing temperature raises the concentration of oxygen vacancy and free electrons.[78] A remaining question is how an increase in the concentrations of oxygen vacancies and electrons deteriorate PV performance of PSCs. There are several studies showing that donor impurities such as Nb increases the electron concentration and improves the charge collection efficiency of PSCs.[79] Based on recent studies, we speculate that the oxygen vacancy is responsible for the decreased PV performance of TiO_2 film grown at high temperature. To understand the role of the oxygen vacancy, J-V curves in Figure 5.7 (b) are fitted using a stand diode equation of solar cells. Figure 5.7 (b) shows the shunt resistance of the PSCs as function of the oxidation temperature. An increase in the annealing temperature decreases the shunt resistance.
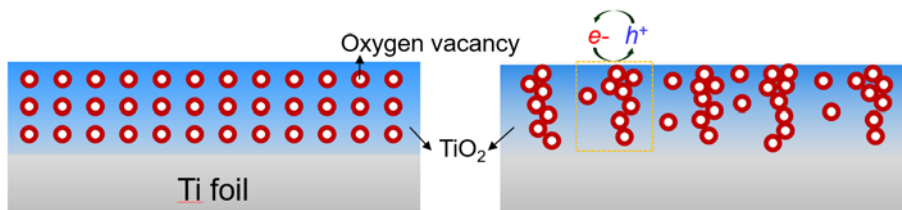
Figure 5.8. Oxygen configuration of oxidized TiO_2 at 400 °C (left) and 700 °C (right).

39

We postulate that a change in the shunt resistance is related to the inhomogeneous agglomeration of oxygen vacancy in TiO_2 film by electric field which is applied during J-V measurement. Hwang et al. have experimentally proven the alignment of the oxygen vacancies in TiO_2 film and its effect on the electric property by combining TEM analysis and electric characterization.[80] Although the oxidized layer thickness of Ti metal foils is same for all samples, higher annealing temperature increase the oxygen vacancy concentration and promotes the agglomeration of the oxygen vacancies in TiO_2 layer under electric field. The formation of the oxygen vacancy filament is illustrated in an inset of Figure 5.8.[81] Once the filament of the oxygen vacancies is formed, there is a shortcut for the electron transport. As the oxygen vacancy concentration increases, the kinetic energy barrier for the formation of the electron path decreases. Consequently, when high temperature annealed TiO_2 layer is used, the leakage current through TiO_2 layer increases and the shunt resistance of PSCs decreases.
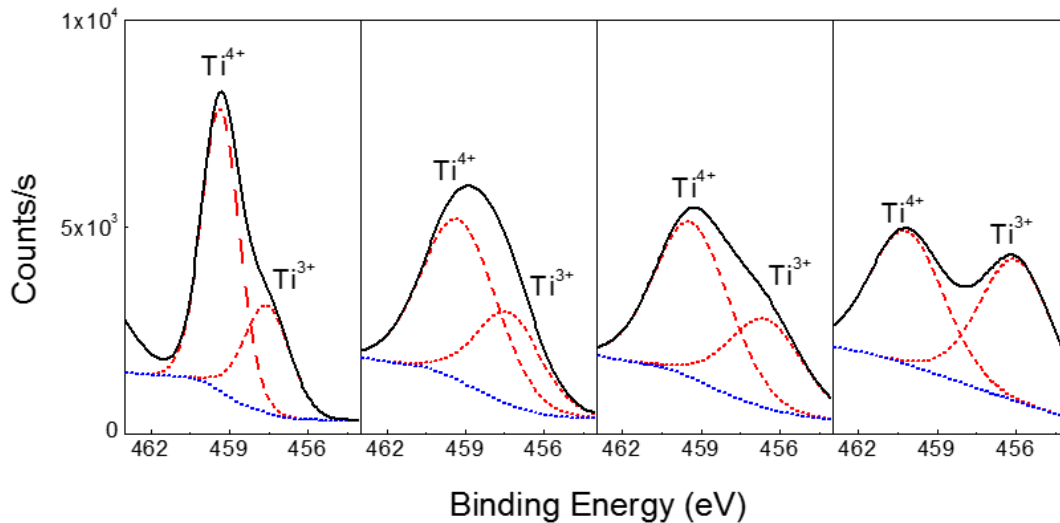
Figure 5.9. XPS spectra of the TiO_2 layer according to different oxidization temperature in air.

To examine the relative oxygen vacancy concentration, XPS analysis was performed for TiO_2 layers. Figure 5.9 shows Ti 2p spectra. Between two peaks, a peak at the binding energy of

~459.2 eV is assigned to Ti4+.[82] The other peak of lower binding energy (457.5 eV) is due to a presence of Ti3+ which is the Ti-defect site associated with oxygen vacancies or other donor impurities.[82] The XPS analysis clearly indicates that an increase in the thermal oxidation temperature also increases the amount of oxygen vacancy which easily agglomerates to form the inhomogeneous path for the electron transport.

5.3.4 Additional Oxidation

To further understand the effect of the oxygen vacancy, TiO_2 layer, which was thermally grown at 400 °C for 72h in air, was additionally treated in oxygen atmosphere at 400 °C. Since the second annealing was conducted for a short time in comparison to the first annealing, the second annealing has little impact on the oxidation of Ti foil. During the second annealing in pure oxygen atmosphere, oxygen atoms preferentially diffuse into TiO_2 layer through a vacancy-assisted diffusion. As a result of oxygen inward diffusion, oxygen vacancies are expected to leave TiO_2 layer by oxygen annealing. A hypothesis on the decrease in the oxygen vacancy is verified by measuring the resistivity of two-time thermal treated Ti substrate. As shown in Figure 5.10, the TiO_2 layer exhibits larger resistance and more non-linear J-V curve after the TiO_2 layer was retreated in oxygen for 1 hr. Moreover, the second treatment almost removed the Ti3+ peak at 457.5 eV in Ti 2p spectra in Figure 5.10 (b).
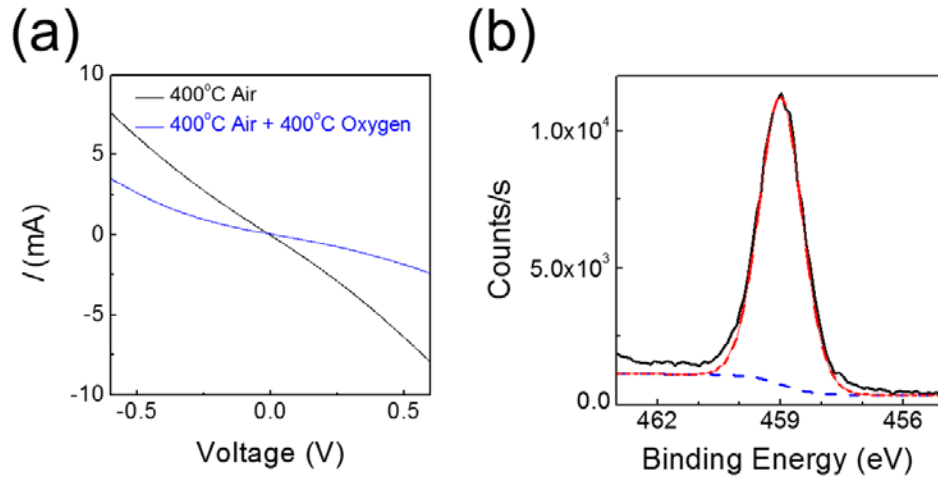
Figure 5.10. (a) The resistance of oxidized TiO_2 layer at 400 °C for 72h on Ti foil with/without second annealing at 400 °C for 1h in oxygen ambient. (b) XPS spectra of oxidized TiO_2 layer on Ti foil after second annealing process.

5.4   STATIC PHOTOVOLTAIC MEASUREMENT

5.4.1   Photovoltaic Measurement
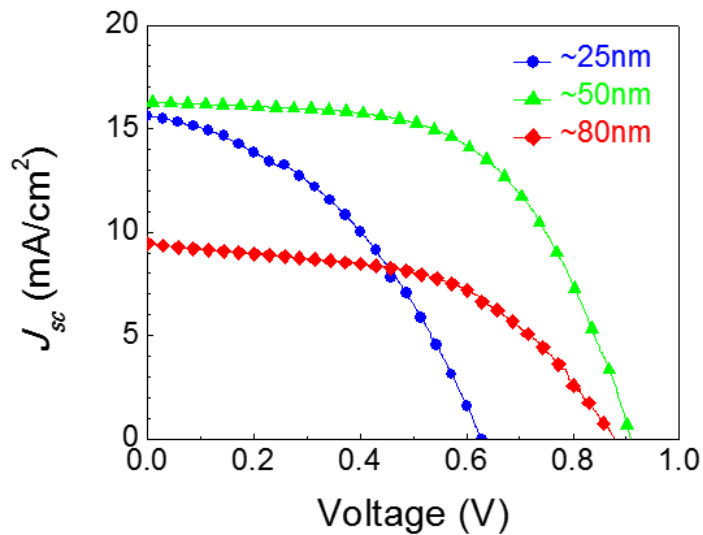
Figure 5.11. *J-V* curves of the flexible perovskite solar cell device fabricated via oxidation in air depending on different thickness under AM 1.5G illumination. The inset plots show each average of the fabricated samples. The thickness is measured by epllisometer.

42

Firstly, to find the optimal thickness of the TiO_2 layer for PSCs, we fabricated flexible PSCs using the Ti foils that were annealed at 400 °C for different oxidation time. Since Ti metal plate at the bottom of PSCs was not transparent, the photovoltaic measurement of PSCs was conducted in a top illumination mode. Current density - voltage (J-V) curve of Ti foil based PSCs is compared as a function of the thickness, as shown in Figure 5.11. When the thickness of TiO_2 on Ti foil is ~50 nm, PSC exhibits the best PCE of ~8.56% with higher Voc and FF in Table 5.1.

Table 5.1. Parameters of the flexible perovskite solar cell device fabricated via oxidation in air depending on different thickness under AM 1.5G illumination.

Thickness (nm)	J_{SC} (mA/cm2)	V_{OC} (V)	FF	Efficiency (%)
~25	15.6	0.66	0.41	4.24
~50	16.2	0.91	0.58	8.56
~80	9.5	0.88	0.52	4.45

A thinner TiO_2 layer on Ti decreases the shunt resistance, which lowered ff, Voc. As a result, the efficiency of PSCs was only ~4.2%. On the other hand, a thicker TiO_2 significantly decreases Jsc, which is attributed to an increase in the series resistance. Therefore, the thickness of the oxidized TiO_2 layer in following experiments was fixed at 50 nm.
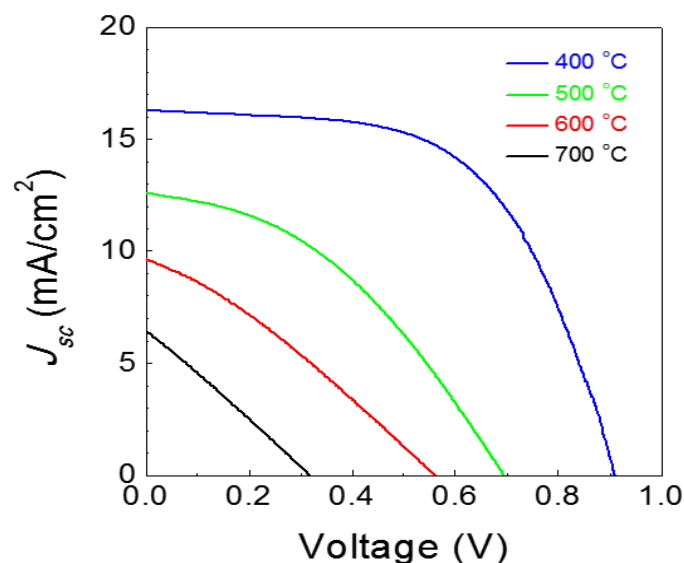
Figure 5.12. J-V curves of Au/Cu/HTM/CH$_3$NH$_3$PbI$_3$ /TiO$_2$/Ti cells under 100 mW cm^{-2} AM1.5G solar light with the same oxidized thickness of TiO$_2$ layer, ~50 nm, based on the same ambience, air, with different annealing temperature.

Figure 5.12 shows J-V curves of PSCs on Ti foils that were annealed at different temperature, but had ~50 nm thick TiO$_2$ layer. By changing thermal annealing time at different temperature, we changed only the crystalline quality of TiO$_2$ layer with the film thickness fixed at 50 nm. To grow 50 nm thick TiO$_2$ layer, Ti foil was annealed at 400 °C for 72 hours, 500 °C for 50 minutes, 600 °C for 8 minutes or 700 °C for 50 seconds. All photovoltaic parameters of flexible perovskite solar cells based on oxidized Ti substrate are shown in Table 5.2.

Table 5.2. Parameters of the flexible perovskite solar cell device fabricated via oxidation in air depending on different temperatures with same thickness, 50 nm, under AM 1.5G illumination.

Temperature (°C)	J$_{SC}$ (mA/cm^2)	V$_{OC}$ (V)	FF	Efficiency (%)
400	16.2	0.91	0.58	8.56

Table 5.2. (continued)

500	12.6	0.70	0.40	3.53
600	9.64	0.56	0.30	1.63
700	6.46	0.32	0.26	0.54

To ensure the reproducibility of the results, over 50 separate devices were fabricated and tested using the optimized Ti oxide thickness of 50 nm. Histogram of the photovoltaic performance characteristics are shown in Figure 5.13.
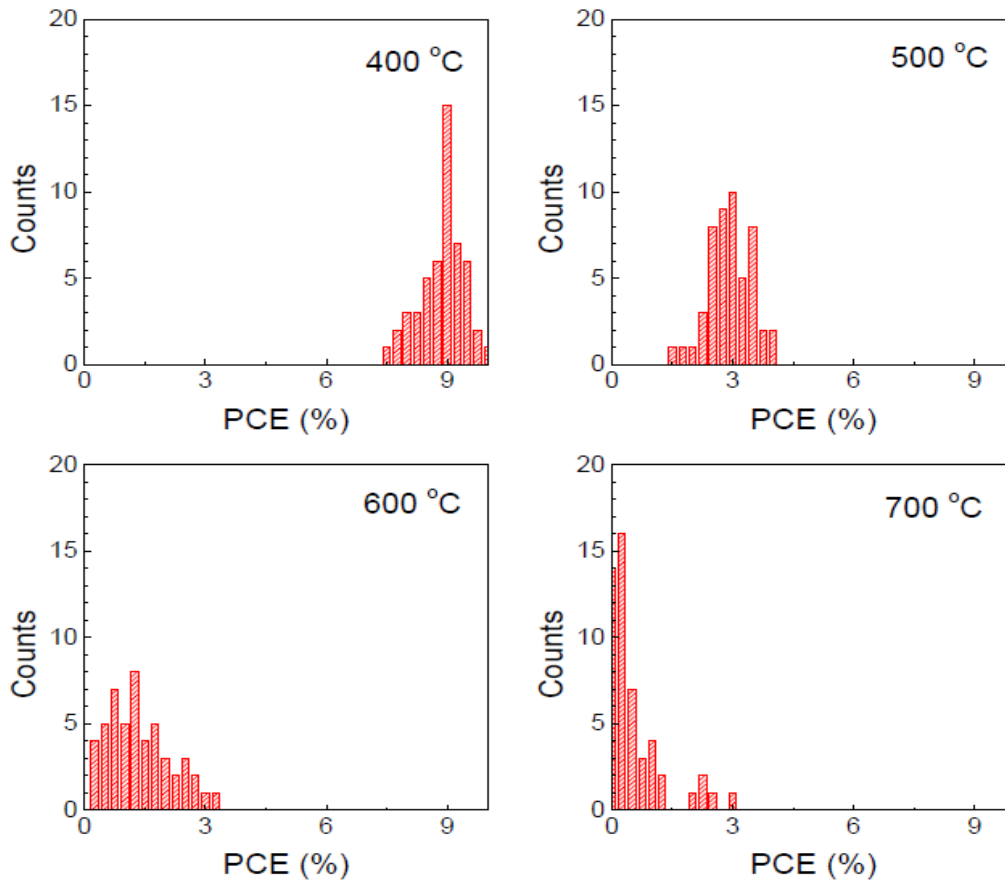
Figure 5.13. Histogram of the power conversion efficiency of oxidized Titanium foil based PSCs (Au/Cu/HTM/CH₃NH₃PbI₃/TiO₂/Ti) at different temperature (400 °C, 500 °C, 600 °C, 700 °C). 50 devices were tested for the statistics.

45

PSCs on 400 °C oxidized Ti foil shows the average PCE of 8.56%. Jsc, Voc, and ff of this PSC are 16.2 mA/cm2, 0.91 V, and 0.58, respectively. The relatively small Jsc of the best PSC is due to the loss of incident light at the top transparent electrode and the HTL in Figure 5.1. Transmittance of the thin metal electrode ranges from 60 to 80 % for visible light. In addition, since HTL (spiro-OMeTAD) is coated on the top of the perovskite layer, HTL captures solar light of the wavelength smaller than ~420 nm.[67] An increase in the annealing temperature decreases PCE and shunt resistance of PSCs, thought the thickness of TiO_2 layer is same for all samples.

5.4.2   J-V Curve and DC Mode IPCE after Additional Oxidation
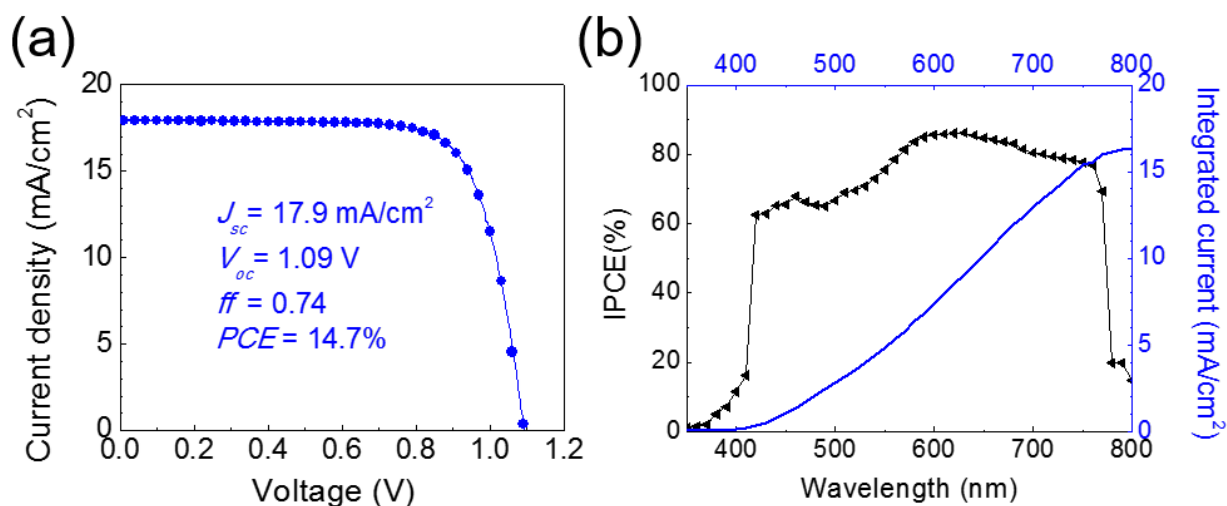
Figure 5.14. (a) *J-V* characteristics measured under 100 mW cm^{-2} AM1.5G illumination for the highest-performing of Au/Cu/HTM/CH$_3$NH$_3$PbI$_3$ /TiO$_2$/Ti device after second annealing at 400 °C for 1 hour in oxygen. (b) IPCE spectrum with the highest-performing device. The integrated product of the IPCE spectrum with the AM1.5G photon flux is also shown (blue line) under the same condition.

Figure 5.14 (a) shows J-V curve of the PSC built on the two-time treated Ti foil under solar light radiation. After the oxygen vacancy concentration is reduced in the TiO_2 layer on Ti foil, the PSC exhibits the best performance. Jsc, Voc, ff, and a PCE are 17.9 mA/cm2, 1.09 V, 0.74, and 14.9 %, respectively. The ETL property of other TiO_2 layers grown at higher temperature in air is also significantly improved when Ti foils are treated in oxygen at 400 °C for 1 hr, as shown in Figure 5.14. Results in this study demonstrate that the oxygen vacancy plays a critical role in lowering the performance of PSCs and the passivation of defects in the oxidized layer of Ti foil helps to recover the shut resistance of PSCs. Figure 5.14 (b) shows IPCE spectra of the best PSC with a negligible oxygen vacancy concentration in the TiO_2 layer. The integrated of current is ~16.3 mA/cm2 which is in a good agreement with Jsc of J-V curve. IPCE of Ti substrate based PSCs drops to 0% at ~420 nm that is longer than the cut-off wavelength of conventional glass based PSCs (~300 nm). This is because solar light is incident from the top electrode and passes through HTM before light hits the perovskite layer. The absorption of high energy photons by HTM, in turn, limits the theoretical efficiency of PSCs. This explains relatively smaller PCE of PSCs on the oxidized Ti foil. It is also noteworthy that the removal of UV component from solar light may improve the light stability of PSCs, since UV is a major source of light induced aging of halide perovskite.
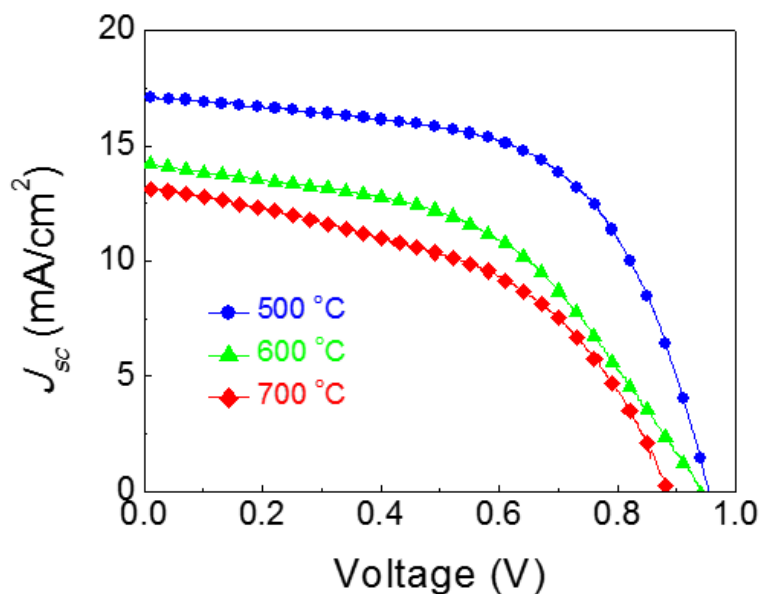
Figure 5.15. Representative *J-V* characteristics of Au/Cu/HTM/CH$_3$NH$_3$PbI$_3$/TiO$_2$/Ti measured under 100 mW cm^{-2} AM1.5G illumination after second annealing at 400 °C for 1h in oxygen ambience.

As shown above J-V characteristics in Figure 5.15, second treatment of TiO$_2$ in different temperatures also decreased oxygen vacancy concentration, resulting in improvement of performances on each oxidized TiO$_2$ in different temperatures.

Table 5.3. Parameters of Au/Cu/HTM/CH$_3$NH$_3$PbI$_3$/TiO$_2$/Ti measured after additional annealing in oxygen at 400 °C for 1h under AM 1.5G illumination.

Temperature (°C)	J$_{SC}$ (mA/cm^2)	V$_{OC}$ (V)	FF	Efficiency (%)
400	17.9	1.09	0.74	14.7
500	17.1	0.95	0.60	9.07
600	14.2	0.94	0.49	6.58
700	13.1	0.89	0.48	6.11

5.5   MECHANICAL PROPERTY

One of the most attractive features of Ti foil based PSCs is that the solar cell is very flexible. We characterized the mechanical strength of Ti foil based PSCs by repeatedly bending PSCs at different radii of curvature (R). Previously, the flexible perovskite solar cells have been studied using polymer substrates such ITO/PEN substrates. It was found that cracking of ITO transparent electrode was a source of degradation of photovoltaic performance. Even at R ~4 mm, PCE of PSCs on ITO/PEN decreases by approximately 50 % after the bending was repeated 1000 times.[10]
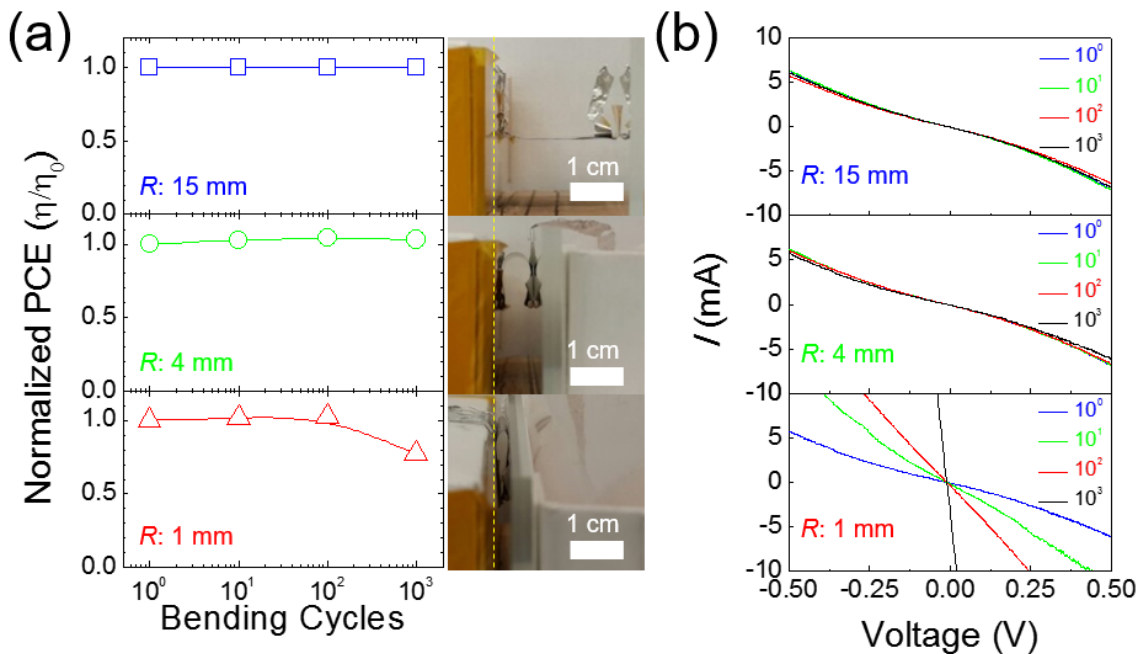
Figure 5.16. (a) Changes in normalized PCEs of flexible perovskite solar cells based on Ti foil during repeated bending cycles, 10, 100, and 1000 cycles, at different bending radius of 15, 4, and 1mm. The inset gives a real photograph of the bending tests. (b) The electrical resistance measured from I-V curve of the Au/TiO2/Ti device before and after 10, 100, and 1000 bending cycles at different bending radius.

Figure 5.16 (a) shows a change in normalized PCE while PSCs are bent 1000 times. Surprisingly, the Ti foil base PSCs maintain the initial PCE of ~100% at R ~15 and 4 mm while 1000 cycles of the bending experiment is conducted. This is due to high ductility of Ti foil in comparison to transparent metal oxide such as ITO. Even at an extreme bending condition (R ~1 mm), Ti foil based PSCs keep the original PCE till 100 cycles of the bending test. PCE of 1000 times bent PSCs is till as high as 77% of the initial PCE. To find out the origin of the fatigue of foil based PSCs, we also measured the change of I-V curve of surface oxidized Ti foils as a function of bending time in a dark condition. For the electric characterization, the electrode structure of $Au/TiO_2/Ti$ in the inset of Figure 5.7 (a) was used. The resistivity of TiO_2 layer on Ti foil did not change at conditions of R ~ 15 and 4 mm. On the other hand, the resistivity of TiO_2 significantly decreases at the condition of R ~ 1 mm. After the bending test repeated 10 cycles at R ~1 mm, J-V curve stated to change. As a result, TiO_2 layer does not work as ETL and the device exhibits a resistance behavior rather than a diode behavior, as shown in Figure 5.16 (b).
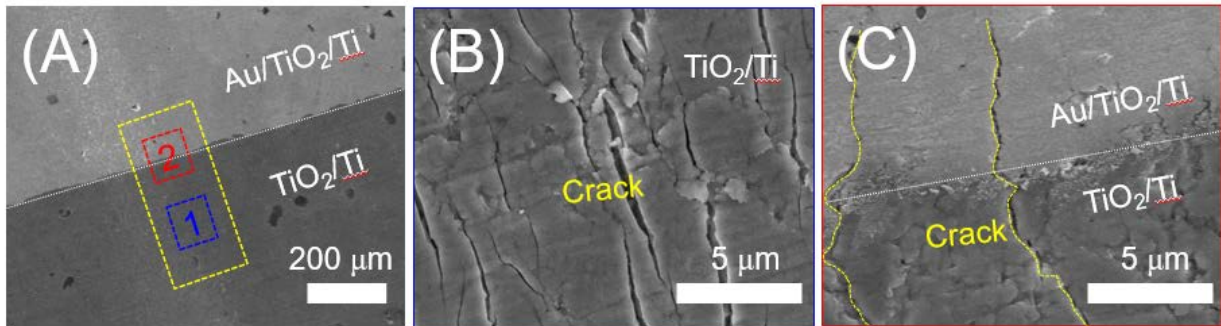
Figure 5.17. Magnified SEM image of the structure of $Au/TiO_2/Ti$ before bending test. (B) and (C) shows magnification SEM images after bending test at 1mm bending radius.

The microstructure of $Au/TiO_2/Ti$ was further investigated using SEM at a plan-view geometry in Figure5.17 (a). Figure 5.17 (b) and (c) shows that the crack produced and the direction of

cracks is perpendicular to the bending direction, after the Ti foil was bent 1000 times at R ~1 mm. The cracks of the surface oxidized Ti foil can cause the degradation of PSCs by generating leakage current through the internal surface of cracks.

6.0   CONCLUSION

I have demonstrated PSCs on the thermally oxidized Ti foil. PCE of PSCs is as high as 14.9 %, though the top illumination through HTM decreases the theoretical efficiency of PSCs by ~8 %). The concentration of oxygen vacancy in the oxidized TiO_2 layer is a very important parameter to control the electric function of TiO_2 as ETL of PSC. The oxygen vacancy forms the bypass of the electron transport and decreases the shunt resistance of PSCs. Moreover, the Ti metal based PSCs exhibit an excellent fatigue resistance during the mechanical bending test. Even at R = 4 mm, the PSCs do not show any decrease in PCE till the bending test is repeated 1000 times. This is better than the fatigue resistance of currently available flexible PSCs on ITO/PET substrates. This suggests that Ti metal based PSCs possess excellent mechanical properties and can be applied to the renewable energy source of wearable electronics.

REFERENCE

[1] Kim, H. S., et al. (2012). "Lead iodide perovskite sensitized all-solid-state submicron thin film mesoscopic solar cell with efficiency exceeding 9%." Sci Rep 2: 591.

[2] Jeon, N. J., et al. (2014). "Solvent engineering for high-performance inorganic-organic hybrid perovskite solar cells." Nat Mater 13(9): 897-903.

[3] Burschka, J., et al. (2013). "Sequential deposition as a route to high-performance perovskite-sensitized solar cells." Nature 499(7458): 316-319.

[4] Ahn, N., et al. (2015). "Highly Reproducible Perovskite Solar Cells with Average Efficiency of 18.3% and Best Efficiency of 19.7% Fabricated via Lewis Base Adduct of Lead(II) Iodide." J Am Chem Soc 137(27): 8696-8699.

[5] Son, D.-Y., et al. (2016). "Self-formed grain boundary healing layer for highly efficient CH3 NH3 PbI3 perovskite solar cells." Nature Energy 1(7): 16081.

[6] Bi, D., et al. (2016). "Polymer-templated nucleation and crystal growth of perovskite films for solar cells with efficiency greater than 21%." Nature Energy 1(10): 16142.

[7] Docampo, P., et al. (2013). "Efficient organometal trihalide perovskite planar-heterojunction solar cells on flexible polymer substrates." Nat Commun 4: 2761.

[8] Liu, D. and T. L. Kelly (2013). "Perovskite solar cells with a planar heterojunction structure prepared using room-temperature solution processing techniques." Nature Photonics 8(2): 133-138.

[9] Qiu, W., et al. (2015). "An electron beam evaporated TiO2layer for high efficiency planar perovskite solar cells on flexible polyethylene terephthalate substrates." J. Mater. Chem. A 3(45): 22824-22829.

[10] Kim, B. J., et al. (2015). "Highly efficient and bending durable perovskite solar cells: toward a wearable power source." Energy Environ. Sci. 8(3): 916-921.

[11] Yang, D., et al. (2015). "High efficiency flexible perovskite solar cells using superior low temperature TiO2." Energy Environ. Sci. 8(11): 3208-3214.

[12] Yin, X., et al. (2016). "Highly Efficient Flexible Perovskite Solar Cells Using Solution-Derived NiOx Hole Contacts." ACS Nano 10(3): 3630-3636.

[13] Jo, J. W., et al. (2016). "Improving Performance and Stability of Flexible Planar-Heterojunction Perovskite Solar Cells Using Polymeric Hole-Transport Material." Advanced Functional Materials 26(25): 4464-4471.

[14] Feng, J. (2014). "Mechanical properties of hybrid organic-inorganic CH3NH3BX3 (B = Sn, Pb; X = Br, I) perovskites for solar cell absorbers." APL Materials 2(8): 081801.

[15] Lee, M., et al. (2016). "Silver Nanowire Top Electrodes in Flexible Perovskite Solar Cells using Titanium Metal as Substrate." ChemSusChem 9(1): 31-35.

[16] Li, Y., et al. (2016). "High-efficiency robust perovskite solar cells on ultrathin flexible substrates." Nat Commun 7: 10214.

[17] Yoon, J., et al. (2017). "Superflexible, high-efficiency perovskite solar cells utilizing graphene electrodes: towards future foldable power sources." Energy Environ. Sci. 10(1): 337-345.

[18] Di Giacomo, F., et al. (2016). "Progress, challenges and perspectives in flexible perovskite solar cells." Energy Environ. Sci. 9(10): 3007-3035.

[19] Troughton, J., et al. (2015). "Highly efficient, flexible, indium-free perovskite solar cells employing metallic substrates." J. Mater. Chem. A 3(17): 9141-9145.

[20] Lee, M., et al. (2015). "Efficient, durable and flexible perovskite photovoltaic devices with Ag-embedded ITO as the top electrode on a metal substrate." J. Mater. Chem. A 3(28): 14592-14597.

[21] Xiao, Y., et al. (2016). "An efficient titanium foil based perovskite solar cell: using a titanium dioxide nanowire array anode and transparent poly(3,4-ethylenedioxythiophene) electrode." RSC Adv. 6(4): 2778-2784.

[22] Perez, R and Perez, M., (2009) "A fundamental look at energy reserves for the planet", The IEA SHC Solar Update, 50: 2.

[23] Jäger-Waldau, A., Monforti-Ferrario, F., Banja, M., Bloem, H., Arantegui, R, L. and Szabo, M., (2012) "PV Status Report 2012", Institute for Energy, Renewable Energy Unit, European Commission.

[24] "Best research cell-efficiency", https://commons.wikimedia.org/wiki/File:Best_Research-Cell_Efficiencies.png

[25] Im, J. H., et al. (2014). "Growth of CH3NH3PbI3 cuboids with controlled size for high-efficiency perovskite solar cells." Nat Nanotechnol 9(11): 927-932.

[26] Kojima, A., et al. (2009). "Organometal Halide Perovskites as Visible-Light Sensitizers for Photovoltaic Cells." Journal of the American Chemical Society 131(17): 6050-6051.

[27] Im, J. H., et al. (2011). "6.5% efficient perovskite quantum-dot-sensitized solar cell." Nanoscale 3(10): 4088-4093.

[28] Lee, M. M., et al. (2012). "Efficient Hybrid Solar Cells Based on Meso-Superstructured Organometal Halide Perovskites." SCIENCE 338(6107): 643.

[29] Liu, M., et al. (2013). "Efficient planar heterojunction perovskite solar cells by vapour deposition." Nature 501(7467): 395-398.

[30] Zhou, H., et al. (2014). "Interface engineering of highly efficient perovskite solar cells." SCIENCE 345(6196): 542.

[31] Mitzi, D. B., et al. (1999). "Thin Film Deposition of Organic−Inorganic Hybrid Materials Using a Single Source Thermal Ablation Technique." Chemistry of Materials 11(3): 542-544.

[32] Chen, C. W., et al. (2014). "Efficient and uniform planar-type perovskite solar cells by simple sequential vacuum deposition." Adv Mater 26(38): 6647-6652.

[33] Song, Z., et al. (2016). "Pathways toward high-performance perovskite solar cells: review of recent advances in organo-metal halide perovskites for photovoltaic applications." Journal of Photonics for Energy 6(2): 022001.

[34] Heo, J. H., et al. (2013). "Efficient inorganic–organic hybrid heterojunction solar cells containing perovskite compound and polymeric hole conductors." Nature Photonics 7(6): 486-491.

[35] Choi, J. J., et al. (2014). "Structure of methylammonium lead iodide within mesoporous titanium dioxide: active material in high-performance perovskite solar cells." Nano Lett 14(1): 127-133.

[36] Leijtens, T., et al. (2013). "Overcoming ultraviolet light instability of sensitized TiO(2) with meso-superstructured organometal tri-halide perovskite solar cells." Nat Commun 4: 2885.

[37] Leijtens, T., et al. (2014). "The Importance of Perovskite Pore Filling in Organometal Mixed Halide Sensitized TiO2-Based Solar Cells." J Phys Chem Lett 5(7): 1096-1102.

[38] Eperon, G. E., et al. (2014). "Morphological Control for High Performance, Solution-Processed Planar Heterojunction Perovskite Solar Cells." Advanced Functional Materials 24(1): 151-157.

[39] Yang, W. S., et al. (2015). "High-performance photovoltaic perovskite layers fabricated through intramolecular exchange." SCIENCE.

[40] Edri, E., et al. (2014). "Why lead methylammonium tri-iodide perovskite-based solar cells require a mesoporous electron transporting scaffold (but not necessarily a hole conductor)." Nano Lett 14(2): 1000-1004.

[41] Jeng, J. Y., et al. (2013). "CH3NH3PbI3 perovskite/fullerene planar-heterojunction hybrid solar cells." Adv Mater 25(27): 3727-3732.

[42] Malinkiewicz, O., et al. (2013). "Perovskite solar cells employing organic charge-transport layers." Nature Photonics 8(2): 128-132.

[43] Dong, Q., et al. (2015). "Abnormal crystal growth in CH3NH3PbI3−xClxusing a multi-cycle solution coating process." Energy Environ. Sci. 8(8): 2464-2470.

[44] Chen, W., et al. (2015). "Efficient and stable large-area perovskite solar cells with inorganic charge extraction layers." SCIENCE 350(6263): 944.

[45] You, J., et al. (2016). "Improved air stability of perovskite solar cells via solution-processed metal oxide transport layers." Nat Nanotechnol 11(1): 75-81.

[46] Chen, W., et al. (2015). "Hybrid interfacial layer leads to solid performance improvement of inverted perovskite solar cells." Energy Environ. Sci. 8(2): 629-640.

[47] Wang, K. C., et al. (2014). "p-type Mesoscopic nickel oxide/organometallic perovskite heterojunction solar cells." Sci Rep 4: 4756.

[48] Park, J. H., et al. (2015). "Efficient CH3 NH3 PbI3 Perovskite Solar Cells Employing Nanostructured p-Type NiO Electrode Formed by a Pulsed Laser Deposition." Adv Mater 27(27): 4013-4019.

[49] Green, M. A., et al. (2014). "The emergence of perovskite solar cells." Nat Photon 8(7): 506-514.

[50] Chen, S., et al. (2017). "Light Illumination Induced Photoluminescence Enhancement and Quenching in Lead Halide Perovskite." Solar RRL 1(1): 1600001.

[51] Jung, H. S. and N. G. Park (2015). "Perovskite solar cells: from materials to devices." Small 11(1): 10-25.

[52] Stranks, S. D., et al. (2013). "Electron-Hole Diffusion Lengths Exceeding 1 Micrometer in an Organometal Trihalide Perovskite Absorber." SCIENCE 342(6156): 341.

[53] Haillant, O. (2011). "Accelerated weathering testing principles to estimate the service life of organic PV modules." Solar Energy Materials and Solar Cells 95(5): 1284-1292.

[54] Kojima, A., et al. (2009). "Organometal Halide Perovskites as Visible-Light Sensitizers for Photovoltaic Cells." Journal of the American Chemical Society 131(17): 6050-6051.

[55] Tiep, N. H., et al. (2016). "Recent Advances in Improving the Stability of Perovskite Solar Cells." Advanced Energy Materials 6(3): 1501420.

[56] Navas, J., et al. (2015). "Revealing the role of Pb(2+) in the stability of organic-inorganic hybrid perovskite CH3NH3Pb1-xCdxI3: an experimental and theoretical study." Phys Chem Chem Phys 17(37): 23886-23896.

[57] Habisreutinger, S. N., et al. (2014). "Carbon nanotube/polymer composites as a highly stable hole collection layer in perovskite solar cells." Nano Lett 14(10): 5561-5568.

[58] Noorden, R, V. (2014). "Cheap solar cells tempt business." Nature 513: 470.

[59] Bella, F., et al. (2016). "Improving efficiency and stability of perovskite solar cells with photocurable fluoropolymers." SCIENCE.

[60] Zhou, Y., et al. (2015). "Room-temperature crystallization of hybrid-perovskite thin films via solvent–solvent extraction for high-performance solar cells." J. Mater. Chem. A 3(15): 8178-8184.

[61] Zhang, H., et al. (2016). "Pinhole-Free and Surface-Nanostructured NiOx Film by Room-Temperature Solution Process for High-Performance Flexible Perovskite Solar Cells with Good Stability and Reproducibility." ACS Nano 10(1): 1503-1511.

[62] Snaith, H. J. (2013). "Perovskites: The Emergence of a New Era for Low-Cost, High-Efficiency Solar Cells." The Journal of Physical Chemistry Letters 4(21): 3623-3630.

[63] Mahan, John E. (2000). "Physical vapor deposition of thin films." Physical Vapor Deposition of Thin Films, by John E. Mahan, pp. 336. ISBN 0-471-33001-9. Wiley-VCH, January 2000. 1.

[64] "The Multispectral Sun, from the National Earth Science Teachers Association". Windows2universe.org. 2007-04-18. Retrieved 2012-02-12

[65] Kayes, Brendan M., et al. (2011). "27.6% Conversion efficiency, a new record for single-junction solar cells under 1 sun illumination." Photovoltaic Specialists Conference (PVSC), 2011 37th IEEE.

[66] Chen, B., et al. (2016). "Efficient Semitransparent Perovskite Solar Cells for 23.0%-Efficiency Perovskite/Silicon Four-Terminal Tandem Cells." Advanced Energy Materials 6(19): 1601128.

[67] Noh, J. H., et al. (2013). "Nanostructured TiO2/CH3NH3PbI3 heterojunction solar cells employing spiro-OMeTAD/Co-complex as hole-transporting material." Journal of Materials Chemistry A 1(38): 11842.

[68] Pantel, R., et al. (1987). "Oxygen behavior during titanium silicide formation by rapid thermal annealing." Journal of Applied Physics 62(10): 4319-4321.

[69] Bernardi, M. I. B., et al. (2001). "TiO2 thin film growth using the MOCVD method." Materials Research 4: 223-226.

[70] Bousoulas, P., et al. (2016). "Engineering amorphous-crystalline interfaces in TiO2−x/TiO2−y-based bilayer structures for enhanced resistive switching and synaptic properties." Journal of Applied Physics 120(15): 154501.

[71] Zhang, H., et al. (2016). "Mg-doped TiO2boosts the efficiency of planar perovskite solar cells to exceed 19%." J. Mater. Chem. A 4(40): 15383-15389.

[72] Kim, D. H., et al. (2015). "Niobium Doping Effects on TiO2 Mesoscopic Electron Transport Layer-Based Perovskite Solar Cells." ChemSusChem 8(14): 2392-2398.

[73] Feng, X., et al. (2009). "Tantalum-doped titanium dioxide nanowire arrays for dye-sensitized solar cells with high open-circuit voltage." Angew Chem Int Ed Engl 48(43): 8095-8098.

[74] Giordano, F., et al. (2016). "Enhanced electronic properties in mesoporous TiO2 via lithium doping for high-efficiency perovskite solar cells." Nat Commun 7: 10379.

[75] Qin, P., et al. (2014). "Yttrium-substituted nanocrystalline TiO(2) photoanodes for perovskite based heterojunction solar cells." Nanoscale 6(3): 1508-1514.

[76] Pathak, S. K., et al. (2014). "Performance and Stability Enhancement of Dye-Sensitized and Perovskite Solar Cells by Al Doping of TiO2." Advanced Functional Materials 24(38): 6046-6055.

[77] Gurylev, V., et al. (2015). "Surface reconstruction, oxygen vacancy distribution and photocatalytic activity of hydrogenated titanium oxide thin film." Journal of Catalysis 330: 177-186.

[78] Pan, X., et al. (2013). "Defective TiO2 with oxygen vacancies: synthesis, properties and photocatalytic applications." Nanoscale 5(9): 3601-3614.

[79] Kim, D. H., et al. (2015). "Niobium Doping Effects on TiO2 Mesoscopic Electron Transport Layer-Based Perovskite Solar Cells." ChemSusChem 8(14): 2392-2398.

[80] Hwang, Y. J., et al. (2009). "High density n-Si/n-TiO2 core/shell nanowire arrays with enhanced photoactivity." Nano Lett 9(1): 410-415.

[81] Claire, A. D. L. (1963). "The analysis of grain boundary diffusion measurements." British Journal of Applied Physics 14(6): 351.

[82] Rafieian, D., et al. (2015). "Controlled formation of anatase and rutile TiO2 thin films by reactive magnetron sputtering." AIP Advances 5(9): 097168.